DETERMINATION OF THE ELASTIC CONSTANTS OF β-CARBON MONOXIDE BY BRILLOUIN SPECTROSCOPY

PETER H. GAMMON


CENTRE FOR NFLD. STUDIES
MAY 8 1979
MEMORIAL UNIVERSITY
OF NEWFOUNDLAND

DETERMINATION OF THE ELASTIC CONSTANTS OF β - CARBON MONOXIDE BY BRILLOUIN SPECTROSCOPY

by

Peter H. Gammon

A thesis submitted in partial fulfillment
of the requirements for the degree of
Master of Science

Department of Physics
Memorial University of Newfoundland

January 1978

St. John's Newfoundland

ABSTRACT

Brillouin spectroscopy has been used to determine the adiabatic elastic constants for the hexagonal close-packed (β) phase of solid carbon monoxide near the triple point. In units of 10^9 N/M^2, the elastic constants were found to be:

$c_{11} = 1.909$ $c_{12} = 1.151$ $c_{13} = .955$

$c_{33} = 2.104$ $c_{44} = .356$

Each of the above values is subject to an uncertainty of about 4%. However, most of this error is included in a multiplicative factor common to all five elastic constants, and uncertainties of less than 1% remain if this factor is divided out. The elastic constants were calculated from experimental data consisting of 35 Brillouin spectra showing various combinations of the longitudinal and the first and second transverse Brillouin components. The spectra were obtained by using a triple-pass Fabry-Perot interferometer to analyze laser light scattered by a single crystal of β - carbon monoxide with a known orientation. The crystal orientations were established from Laue x-ray diffraction photographs, and a fully algebraic procedure for interpreting the photographs has been developed and described in considerable detail. Derived elastic properties, in particular, bulk modulus, linear compressibility, and Young's modulus, have been calculated for β - CO and the values have been compared with those of four other materials having hexagonal crystal symmetry. A high degree of similarity was observed when comparing the elastic properties of β - CO with those of β - N_2.

ACKNOWLEDGEMENTS

I would like to express my sincere gratitude to Dr. H. Kiefte and Dr. M. J. Clouter for suggesting this project and for granting me the use of their excellent experimental facilities. Their advice and assistance throughout the experimental work and the writing of this thesis is much appreciated. My thanks are also extended to Professor A. E. Fekete, who scrutinized the mathematics in the chapter on crystal orientation. As well, I am grateful to Miss Carol Butler for typing this thesis. While conducting this research, I was supported by a National Research Council of Canada 1967 Science Scholarship for which I am most thankful.

TABLE OF CONTENTS

LIST OF FIGURES AND TABLES

CHAPTER 1

INTRODUCTION AND THEORY

1.1 Introduction

When carbon monoxide is cooled through its triple point, 68.15 K, it forms a solid phase having a hexagonal close-packed crystal structure. This solid phase is referred to as β-CO and persists for only a short temperature range, 6.5 K, after which transition to a face centred cubic phase, α-CO, occurs. β-carbon monoxide, with which the present work is concerned, is typical of a class of materials characterized by low melting points, high compressibilities, and other physical properties indicative of the relatively weak van der Waals forces which bind their crystal lattices. Several such van der Waals lattices, in particular the rare gas solids, Ne, Ar, Kr, Xe (McLaren et al., 1975; Gewurtz and Stoicheff, 1974; Landheer et al., 1976; Gornall and Stoicheff, 1971) along with some diatomic molecular crystals, O_2, N_2 (Kiefte and Clouter, 1975, 1976) and H_2 (Thomas et al., 1977) have recently been the subject of experiments aimed at determining their elastic properties. The relevance of these experiments stems primarily from the fact that the elastic properties of a crystal are strongly dependent on the potential function with which the molecules constituting the crystal interact. Thus, a hypothesized intermolecular potential function can be subjected to a very sensitive test by using it to derive elastic properties and then comparing the derived properties with those obtained by experiment. An example of this procedure, carried out for the case of β-nitrogen, is found in the paper by Goldman and Klein (1976).

The work to be described in the following chapters represents the first known determination of the elastic properties of β-carbon monoxide. The experimental method used was Brillouin spectroscopy, this method having also been applied to each of the seven substances referred to in the previous paragraph. The inherently passive nature of a Brillouin scattering experiment (a beam of light is all that is required to probe the sample) makes it a particularly suitable technique for dealing with the very delicate and inaccessible van der Waals type of crystals.

β-carbon monoxide was chosen for the present investigation for a number of reasons. Firstly, of the two solid phases of carbon monoxide, it is by far the easier to obtain as a single crystal (only by using samples which are good quality single crystals can the complete set of elastic properties of a substance be determined from Brillouin scattering experiments). Secondly, carbon monoxide itself is a particularly interesting substance for study. Like the various materials mentioned above, its molecular and crystal structure are both relatively simple, thus making experimentally obtained results especially useful from a theoretical viewpoint. An additional feature of carbon monoxide is the relatively small separation in temperature between the triple point and the β-α phase transition. This will very probably allow the investigation of the elastic properties of CO to be continued into the α phase, particularly in the region of the β-α phase transition. Such an investigation has not been conducted before.The usual difficulty encountered in this type of experiment lies in the fact that large thermal expansion effects very often cause disintegration of single crystals (for an example of this effect, in neon, see the thesis by McLaren, 1973) when they are subjected

to temperature variations. Present experimental technique allows single crystals to be grown only from the liquid. Therefore, Brillouin investigation of lower temperature solid phases requires cooling of single crystals and is practical only if the crystals have a reasonable probability of surviving intact. Because of the small temperature change required, the probability of survival of carbon monoxide crystals is likely greater than that for any other van der Waals lattice. A discussion of some of the theoretical relations between elasticity and solid-solid phase transitions can be found in Born and Huang (1954). It is hoped that future results from experiments on carbon monoxide will shed additional light on this topic.

Another particular point of interest in studying carbon monoxide results from its similarity to nitrogen. Apart from the fact that the two materials are isoelectronic and have virtually identical molecular weights, there are, as well, striking similarities in their thermodynamic properties. The two substances have molar volume vs. temperature curves (at equilibrium vapour pressure) which are nearly coincident for temperatures less than 20 K and greater than 70 K (curves for both N_2 and CO are given in a paper by Fukushima, Gibson and Scott, 1977). In the intermediate range, nitrogen, like CO first solidifies in a hcp β phase, and then, upon cooling, undergoes transition to a fcc α phase. In nitrogen, however, the β-α phase transition lies 27.6 K below the triple point and is therefore not nearly so accessible to investigation by Brillouin scattering as is the case with CO. Further similarity in the thermodynamic properties of CO and N_2 is indicated by a complicated equation of state for liquid and gaseous carbon monoxide given by Hust and Stewart (1963). The equation

was derived by adjusting parameters in a theoretically justified equation of state for N_2, and was found to be accurate for CO over a wide range of temperatures and pressures.

In view of the similarities noted above, it would seem reasonable to anticipate a significant degree of correlation in the elastic properties of CO and N_2. This, in turn should allow one to gain additional insight into the molecular interactions in each material by attempting to account for the various differences which are observed to occur. At present, virtually no theory relating directly to β-CO can be found in the literature. However, both the α and β phase of N_2 have been the subject of considerable theoretical investigation (for detailed discussion and an extensive list of references, see the review paper by Scott, 1976). It was therefore decided that a comparison of the elastic properties of N_2 (as determined by Kiefte and Clouter, 1976) and CO should form an important part of the analysis of the data obtained in the present experiment. This comparison, however, is limited primarily to listing the similarities and differences in certain elastic properties, and does not offer interpretations or explanations. It is hoped that the points noted will be of value in future theoretical analysis.

Finally, a word of introduction should be said regarding the second chapter in this thesis. This chapter is involved entirely with the problem of establishing the orientation of single crystals. The theory discussed in chapter two enabled development of a streamlined crystal orientation procedure which was of great advantage in handling the large number of orientations necessary in the present investigation. The generality of the treatment, while increasing the efficiency of the

procedure required for this experiment, provides the additional benefit of making the results useable under a variety of other experimental circumstances. The approach described appears to be original in that no similar, general treatment of the problem could be found in the literature.

1.2 Stress, Strain and Elastic Constants

The classical theory of elasticity in crystals deals with mechanical deformations which extend over a sufficient number of unit cells to enable a crystal to be treated as a continuous medium. The range of intermolecular forces within the crystal is taken to be zero and body forces are neglected. Hence, the only forces which act on a given internal volume element are surface forces originating from immediately adjacent volume elements. Let $\vec{F} \equiv (F_1, F_2, F_3)$ denote the total force acting on a volume element V. Since each component F_i of $\vec{F}$ results entirely from forces acting on the surface, S, of V, it is possible to express F_i as an integral over S. The general form of such an integral is,

$$F_i = \oint_S \vec{\sigma}_i \cdot d\vec{a} \qquad 1\text{-}1$$

where $d\vec{a}$ is an element of surface area directed along the outward normal to V and $\vec{\sigma}_i \cdot d\vec{a}$ is the component of force in the i'th direction acting on $d\vec{a}$. Writing the vectors on the right hand side of 1-1 in terms of their components yields:

$$F_i = \oint_S \sum_{j=1}^{3} \sigma_{ij}\, d\, a_j \qquad 1\text{-}2$$

The quantities σ_{ij} form a three by three matrix which transforms under a coordinate rotation as a second rank tensor (Nye, 1957, p. 87). This matrix is referred to as the stress tensor.

The physical meaning of the σ_{ij} can be seen by considering a unit element of surface area normal to coordinate axis j. σ_{ij} is then the i'th component of the force acting on this element. The σ_{ij} have

units of pressure.

Applying the divergence theorem to 1-1 enables F_i to be expressed as an integral over V. That is:

$$F_i = \int_V \nabla \cdot \vec{\sigma}_i \, dV$$

i.e.

$$F_i = \int_V \sum_{j=1}^{3} \frac{\partial \sigma_{ij}}{\partial x_j} \, dV \qquad 1\text{-}3$$

writing F_i in terms of a force per unit volume or force density, f_i, yields:

$$F_i = \int_V f_i \, dV \qquad 1\text{-}4$$

Comparison of equations 1-3 and 1-4 then implies:

$$f_i = \sum_{j=1}^{3} \frac{\partial \sigma_{ij}}{\partial x_j} \qquad 1\text{-}5$$

By calculating the torque, $\vec{T}$, acting on a given volume element, it is possible to show that σ_{ij} is a symmetric tensor. By definition:

$$\vec{T} = \int_V \vec{r} \times \vec{f} \, dV \qquad 1\text{-}6$$

Let T_1 denote the x_1 component of $\vec{T}$. Then:

$$T_1 = \int_V (x_2 f_3 - x_3 f_2) \, dV$$

Using equation 1-5:

$$T_1 = \int_V \sum_{j=1}^{3} \left(x_2 \frac{\partial \sigma_{3j}}{\partial x_j} - x_3 \frac{\partial \sigma_{2j}}{\partial x_j}\right) dV$$

$$T_1 = \int_V \sum_{j=1}^{3} \frac{\partial}{\partial x_j} (x_2 \sigma_{3j} - x_3 \sigma_{2j}) \, dV$$

$$- \int_V \sum_{j=1}^{3} \left(\sigma_{3j} \frac{\partial x_2}{\partial x_j} - \sigma_{2j} \frac{\partial x_3}{\partial x_j}\right) dV$$

Expressing the first term on the right above as a surface integral, using the divergence theorem, and evaluating the second term, yields:

$$T_1 = \oint_S \sum_{j=1}^{3} (x_2 \sigma_{3j} - x_3 \sigma_{2j}) \, da_j$$
$$- \int_V (\sigma_{32} - \sigma_{23}) \, dV \qquad 1\text{-}7$$

Since any torque on V must result entirely from forces acting on its surface, the volume integral will be identically zero. Thus, since V is arbitrary:

$$\sigma_{32} = \sigma_{23} \qquad 1\text{-}8$$

An identical argument using the x_2 and x_3 components of $\vec{T}$ shows,

$$\sigma_{13} = \sigma_{31}$$
$$\text{and} \qquad \sigma_{12} = \sigma_{21} \qquad 1\text{-}8$$

respectively.

It is now necessary to examine the deformation induced in a crystal by the action of a given stress. With respect to a cartesian coordinate system fixed in space, let $\vec{r} \equiv (r_1, r_2, r_3)$ denote the position of an arbitrary point anchored in a stress-free crystal lattice. When stress is applied this point will move to a new location, $\vec{r}' = \vec{r} + \vec{u}(\vec{r})$ where $\vec{u}(\vec{r})$ is a vector valued function of the original coordinates of the point. In general, the function $\vec{u}(\vec{r})$ will contain information not only on the distortion of volume elements within the crystal, but also on changes in their position and orientation. The key information, namely

that relating to the distortion, can be isolated from the function $\vec{u}(\vec{r})$ by considering changes in distance between nearby points. Let $d\vec{r}$ be the vector joining two points prior to the deformation and let $d\vec{r}' \equiv d\vec{r} + d\vec{u}$ be the vector joining them afterwards. Then:

$$dr'^2 = dr^2 + 2 \sum_{i=1}^{3} dr_i \, du_i + du^2 \qquad 1\text{-}9$$

If it is now assumed that the magnitude of the displacement vector, du, is small compared to the original distance between the points, dr, then the final term on the right of equation 1-9 can be neglected (Landau and Lifshitz, 1959, p. 3). Thus:

$$dr'^2 = dr^2 + 2 \sum_{i=1}^{3} dr_i \, du_i$$

$$\therefore \quad dr'^2 = dr^2 + 2 \sum_{i=1}^{3} dr_i \left(\sum_{j=1}^{3} \frac{\partial u_i}{\partial r_j} dr_j \right)$$

$$\therefore \quad dr'^2 - dr^2 = 2 \sum_{i=1}^{3} \sum_{j=1}^{3} \frac{\partial u_i}{\partial r_j} dr_i \, dr_j \qquad 1\text{-}10$$

In the summation on the right above there are only six distinct products of the form $dr_i \, dr_j$ whereas there appear to be nine distinct coefficients, $\frac{\partial u_i}{\partial r_j}$. This situation can be corrected by writing:

$$\frac{\partial u_i}{\partial r_j} = \tfrac{1}{2} \left(\frac{\partial u_i}{\partial r_j} + \frac{\partial u_j}{\partial r_i} \right) + \tfrac{1}{2} \left(\frac{\partial u_i}{\partial r_j} - \frac{\partial u_j}{\partial r_i} \right) \qquad 1\text{-}11$$

Substituting 1-11 into 1-10 yields:

$$dr'^2 - dr^2 = \sum_{i=1}^{3} \sum_{j=1}^{3} \left(\frac{\partial u_i}{\partial r_j} + \frac{\partial u_j}{\partial r_i} \right) dr_i \, dr_j + \sum_{i=1}^{3} \sum_{j=1}^{3} \left(\frac{\partial u_i}{\partial r_j} - \frac{\partial u_j}{\partial r_i} \right) dr_i \, dr_j$$

However, the second term on the right above sums to zero. Therefore,

$$dr'^2 - dr^2 = 2 \sum_{i=1}^{3} \sum_{j=1}^{3} e_{ij}\, dr_i\, dr_j \qquad 1\text{-}12$$

where $e_{ij} \equiv \frac{1}{2}\left(\frac{\partial u_i}{\partial r_j} + \frac{\partial u_j}{\partial r_i}\right)$. The matrix with entries e_{ij} forms a symmetric second rank tensor known as the strain tensor (Musgrave, 1970, p. 14). This tensor completely specifies the distortion of a crystal in the neighbourhood of an arbitrary point. The e_{ij} are ratios of distances and thus are dimensionless.

Experimental evidence suggests that for most crystalline materials, the components of stress and strain are related by a linear transformation. This empirical result is known as Hooke's law and is usually found to be valid when the strain is sufficiently small that only elastic or recoverable deformations of the crystal occur (Landau and Lifshitz, 1959, p. 12). Hooke's law can be written:

$$\sigma_{ij} = \sum_{k=1}^{3} \sum_{l=1}^{3} c_{ijkl}\, e_{kl} \qquad 1\text{-}13$$

The 81 quantities c_{ijkl} are referred to as the elastic stiffness constants of a crystal and form a tensor of rank four (Nye, 1957, p. 133). The elastic constant tensor has substantial symmetry which can be demonstrated using a variety of arguments. Equation 1-13 along with the symmetry of the stress tensor, σ_{ij}, implies:

$$c_{ijkl} = c_{jikl} \qquad 1\text{-}14$$

The symmetry of the strain tensor combined with an argument similar to that used in obtaining equation 1-12 from equation 1-10 enables the c_{ijkl} to be defined such that:

$$c_{ijkl} = c_{ijlk} \qquad 1\text{-}15$$

To show additional symmetry it is necessary to consider the dependence of the elastic potential energy on the elements e_{ij} of the strain tensor. As a first step it is useful to write Hooke's law in the following form:

$$\sigma_{ij} = \left(\sum_{k=1}^{3} c_{ijkk}\, e_{kk}\right) + 2\, c_{ij23}\, e_{23} + 2\, c_{ij13}\, e_{13} + 2\, c_{ik12}\, e_{12}$$

The notation can then be condensed by contracting the subscripts according to the following scheme:

$11 \rightarrow 1$	$23 \rightarrow 4$	
$22 \rightarrow 2$	$13 \rightarrow 5$	1-16
$33 \rightarrow 3$	$12 \rightarrow 6$	

In addition, the factors of 2 are eliminated from the equation for Hooke's law by defining,

$$\varepsilon_{ij} = e_{ij} \quad , \quad i = j$$
$$\varepsilon_{ij} = 2e_{ij} \quad , \quad i \neq j \qquad 1\text{-}16$$

and then contracting the subscripts as described above. Hooke's law then becomes:

$$\sigma_i = \sum_{j=1}^{6} c_{ij}\, \varepsilon_j \qquad 1\text{-}17$$

It can be shown using a simple geometrical argument that the work done on a unit cube by changing ε_j to $\varepsilon_j + d\varepsilon_j$ is given by $dW_j = \sigma_j \, d\varepsilon_j$ (Nye, 1957, p. 136). Hence the work done per unit volume by a change in the strain elements is given by:

$$dW = \sum_{j=1}^{6} \sigma_j \, d\varepsilon_j \qquad 1\text{-}18$$

If this work can be fully recovered by allowing the crystal to return to its original state of strain, a potential energy per unit volume, Φ, can be associated with the deformation. Then:

$$dW = d\Phi \qquad 1\text{-}19$$

combining Hooke's law with equations 1-18 and 1-19 yields:

$$d\Phi = \sum_{i=1}^{6} \sum_{j=1}^{6} c_{ij} \, \varepsilon_j \, d\varepsilon_i \qquad 1\text{-}20$$

Since Φ is a function of the six ε_j'S, d Φ can be expanded as:

$$d\Phi = \sum_{i=1}^{6} \frac{\partial \Phi}{\partial \varepsilon_i} \, d\varepsilon_i \qquad 1\text{-}21$$

Equating the coefficients of d ε_i in equations 1-20 and 1-21 gives:

$$\frac{\partial \Phi}{\partial \varepsilon_i} = \sum_{j=1}^{6} c_{ij} \, \varepsilon_j \qquad 1\text{-}22$$

Then, differentiating both sides of equation 1-22 with respect to ε_i yields:

$$\frac{\partial^2 \Phi}{\partial \varepsilon_i \partial \varepsilon_j} = c_{ij} \qquad 1\text{-}23$$

Finally, since mixed partial derivatives are equal:

$$c_{ij} = c_{ji} \qquad 1\text{-}24$$

In changing back to the four subscript notation, this relation becomes

$$c_{ijkl} = c_{klij} \qquad 1\text{-}25$$

The combination of equations 1-14, 1-15 and 1-25 reduces the number of independent elements of the tensor c_{ijkl} to 21. In actuality, only 18 of these are independent since three may be specified arbitrarily by expressing the stress and strain tensors in a particular coordinate system. (Landau and Lifshitz, 1959, p. 37). Crystal symmetry further reduces the number of independent elastic constants as is shown for the hexagonal case in the next section.

1.3 Elastic Waves in Hexagonal Crystals

Results from the classical theory of elasticity can be used to quantitatively describe the motion of long wavelength elastic waves in a single crystal. The velocity of propagation of these waves depends on the crystal density and the elements, c_{ijkl}, of the elastic stiffness constant tensor. Hence it is possible to infer the values of the tensor elements from measurements of wave propagation velocities. Before deriving the appropriate equations for hexagonal crystals it is first advantageous to use the hexagonal symmetry to simplify the elastic constant tensor as much as possible.

The essential symmetry element possessed by crystals of the hexagonal system is a six-fold rotation axis (Cullity, 1956). Defining this axis to be the z axis in the crystal allows the basic symmetry operation, rotation of $\pi/3$ radians, to be represented by the following matrix:

$$\begin{pmatrix} \frac{1}{2} & \sqrt{3}/2 & 0 \\ -\sqrt{3}/2 & \frac{1}{2} & 0 \\ 0 & 0 & 1 \end{pmatrix} \qquad 1\text{-}26$$

Since a rotation of $\pi/3$ leaves a hexagonal crystal in an orientation indistinguishable from its original orientation, the elements of the elastic constant tensor must remain identical when transformed by the above matrix. Under a coordinate rotation the components of a fourth rank tensor, c_{ijkl}, transform as,

$$c'_{ijkl} = \sum_{m=1}^{3} \sum_{n=1}^{3} \sum_{p=1}^{3} \sum_{q=1}^{3} a_{im}\, a_{jn}\, a_{kp}\, a_{lq}\, c_{mnpq} \qquad 1\text{-}27$$

where the c'_{ijkl} are the tensor elements expressed in the rotated coordinate system and the a_{ij} are entries from the rotation matrix (Musgrave, 1970, p. 30). Substituting the a_{ij} from the matrix 1-26 into equation 1-27 and using the relation,

$$c'_{ijkl} = c_{ijkl} \qquad 1\text{-}28$$

enables one constraint to be placed on the elastic constant tensor for each set of subscripts, i j k l. A typical example, found from transforming the element c_{1111}, would be:

$$c'_{1111} \equiv c_{1111} = 1/16\ c_{1111} + 9/16\ c_{2222} +$$

$$3/8\ c_{1122} + 3/4\ c_{1212} + \sqrt{3}/4\ c_{1112} + 3\sqrt{3}/4\ c_{1222}$$

The combined set of equations of the above type, not all of which are independent, reduces the elastic constant tensor for hexagonal crystals to the form indicated below (Musgrave, 1970, p. 56). Two subscript notation is used for convenience in displaying the tensor elements in matrix format:

$$\begin{pmatrix} c_{11} & c_{12} & c_{13} & 0 & 0 & 0 \\ c_{12} & c_{11} & c_{13} & 0 & 0 & 0 \\ c_{13} & c_{13} & c_{33} & 0 & 0 & 0 \\ 0 & 0 & 0 & c_{44} & 0 & 0 \\ 0 & 0 & 0 & 0 & c_{44} & 0 \\ 0 & 0 & 0 & 0 & 0 & \frac{c_{11}-c_{12}}{2} \end{pmatrix} \qquad 1\text{-}29$$

It can be shown that when the c_{ijkl} are chosen to satisfy

equations 1-27 and 1-28 for the matrix given in 1-26, then these equations will be satisfied by the matrix representing an arbitrary rotation about the z axis.(Musgrave, 1970, p. 43). Thus, the elastic constant tensor retains the same elements regardless of the orientation of the x axis which can therefore be positioned arbitrarily in the x - y plane. This implies the useful result that the elastic properties of a hexagonal crystal show cylindrical isotropy about the six-fold axis. In particular, the propagation velocity of elastic waves depends only on the angle, γ, between their direction of propagation and the six-fold axis of the crystal.

The equation describing wave propagation in a single crystal follows from the application of Newton's second law to an infinitesimal volume element in a crystal with density, ρ. The equation takes the form,

$$\vec{f} = \rho \frac{d^2\vec{u}}{dt^2} \qquad 1\text{-}30$$

where $\vec{f}$ is the force per unit volume as defined in equation 1-4 and $\vec{u}$ is the displacement of the volume element from its equilibrium position (Landau and Lifshitz, 1959, p. 98). Writing the i'th component of equation 1-30 and using equation 1-5 to expand f_i yields:

$$\sum_{j=1}^{3} \frac{\partial \sigma_{ij}}{\partial x_j} = \rho \frac{d^2 u_i}{dt^2} \qquad 1\text{-}31$$

Application of Hooke's law to equation 1-31 then gives:

$$\sum_{j=1}^{3} \sum_{k=1}^{3} \sum_{l=1}^{3} c_{ijkl} \frac{\partial e_{kl}}{\partial x_j} = \rho \frac{d^2 u_i}{dt^2}$$

Using the definition of the strain components, e_{ij}, enables the above equation to be expressed as:

$$\tfrac{1}{2} \sum_{j=1}^{3} \sum_{k=1}^{3} \sum_{l=1}^{3} c_{ijkl} \left(\frac{\partial^2 u_k}{\partial x_j \partial x_l} + \frac{\partial^2 u_l}{\partial x_j \partial x_k} \right) = \rho \frac{d^2 u_i}{dt^2}$$

Since $c_{ijkl} = c_{ijlk}$ and since there is summation over the indices k and l, these indices can be interchanged in the first term in brackets above, thus allowing the two terms to be combined. The wave equation then becomes:

$$\sum_{j=1}^{3} \sum_{k=1}^{3} \sum_{l=1}^{3} c_{ijkl} \frac{\partial^2 u_l}{\partial x_j \partial x_k} = \rho \frac{d^2 u_i}{dt^2} \qquad 1\text{-}32$$

A solution to equation 1-32 is given by the function representing a plane wave of unit amplitude. That is:

$$u_i(\vec{r}, t) = u_{i0} e^{\sqrt{-1}\,(\vec{k} \cdot \vec{r} - \omega t)} \qquad 1\text{-}33$$

Substituting equation 1-33 into equation 1-32, evaluating the derivatives, and simplifying the resultant expression, yields (Landau and Lifshitz, 1959, p. 104):

$$\sum_{j=1}^{3} \sum_{k=1}^{3} \sum_{l=1}^{3} c_{ijkl} k_j k_k u_{l0} = \rho \omega^2 u_{i0}$$

$$\leftrightarrow \quad \sum_{l=1}^{3} \left(\sum_{j=1}^{3} \sum_{k=1}^{3} c_{ijkl} k_j k_k - \rho \omega^2 \delta_{il} \right) u_{l0} = 0$$

that is,

$$A \vec{u}_0 = 0 \qquad 1\text{-}34$$

where A is the square matrix with entries:

$$A_{il} = \sum_{j=1}^{3} \sum_{k=1}^{3} \left(c_{ijkl} k_j k_k - \rho \omega^2 \delta_{il} \right) \qquad 1\text{-}35$$

An equation of the form 1-34 will be satisfied by non-trivial $\vec{u}_0$, only if:

$$|A| = 0 \qquad 1\text{-}36$$

Writing out $|A|$ explicitly yields a third degree polynomial in ω^2, the three roots of which form expressions for ω^2 as a function of the components, k_i, of the wave vector. Each root specifies a particular group velocity for elastic wave propagation. The velocity is given by,

$$v = \frac{\omega}{k} \qquad 1\text{-}37$$

where $k = \sqrt{k_1^2 + k_2^2 + k_3^2}$.

To find the propagation velocities for hexagonal crystals it is convenient to first reduce the elastic constant tensor to the form given in 1-29 and then use the property of cylindrical isotropy to allow positioning of the x axis such that $\vec{k}$ lies in the x - z plane. The k_i's will then be given by,

$$\begin{aligned} k_1 &= k \sin \gamma \\ k_2 &= 0 \\ k_3 &= k \cos \gamma \end{aligned} \qquad 1\text{-}38$$

where γ is the angle between $\vec{k}$ and the z axis. The final expressions for the propagation velocities are then found to be (Musgrave, 1970, p. 95):

$$V_L = \frac{1}{\sqrt{2\,\rho}} \{ c_{11} \sin^2 \gamma + c_{33} \cos^2 \gamma + c_{44} + [(c_{11} \sin^2 \gamma + c_{33} \cos^2 \gamma - c_{44})^2 - 4 \sin^2 \gamma \cos^2 \gamma \times ((c_{11} - c_{44}) (c_{33} - c_{44}) - (c_{13} + c_{44})^2)]^{\frac{1}{2}}\}^{\frac{1}{2}} \qquad 1\text{-}39a$$

$$V_{T1} = \frac{1}{\sqrt{2\,\rho}} \{(c_{11} - c_{12}) \sin^2 \gamma + 2\, c_{44} \cos^2 \gamma\}^{\frac{1}{2}} \qquad 1\text{-}39b$$

$$V_{T2} = \frac{1}{\sqrt{2}\,\rho}\ \{c_{11}\sin^2\gamma + c_{33}\cos^2\gamma + c_{44} - [(c_{11}\sin^2\gamma + c_{33}\cos^2\gamma - c_{44})^2 - 4\sin^2\gamma\cos^2\gamma \times ((c_{11} - c_{44})(c_{33} - c_{44}) - (c_{13} + c_{44})^2)]^{\frac{1}{2}}\}^{\frac{1}{2}} \qquad 1\text{-}39c$$

It can be shown that the displacement vectors $\vec{u}$ associated with the three types of waves, L, T1 and T2, are mutually orthogonal (Landau and Lifshitz, 1959, p. 104). The wave with velocity V_{T1} is a pure transverse wave, that is, $\vec{u}$ and $\vec{k}$ are perpendicular, while the waves having velocities V_L and V_{T2} are only predominantly longitudinal and transverse respectively since each has components of displacement both perpendicular and parallel to $\vec{k}$ (Musgrave, 1970, p. 98).

The phenomenon of Brillouin scattering provides a means of experimentally measuring elastic wave propagation velocities in transparent crystals. An intuitive description of the process comes from considering the following classical argument (more rigorous theoretical treatments of Brillouin scattering can be found in the literature, for example, Benedek and Fritsch, 1966). Since elastic waves produce regions of compression and rarefaction in a crystal, they can be expected to cause fluctuations in the refractive index of the volume through which they pass. Locally, these fluctuations resemble plane surfaces and hence will cause mirror-like reflection of light incident upon them. However, the "mirrors" are moving inside the crystal with the velocity, V, of elastic wave propagation. To an observer viewing the reflected

(scattered) light this motion is indistinguishable from a motion of the light source.

If a reflecting plane moves a distance, d, in a direction normal to its surface, then the physical path that the light must travel changes by 2 d sin(α/2) where α is the angular deviation of a reflected ray from its original path (see figure 1 below). The change in optical

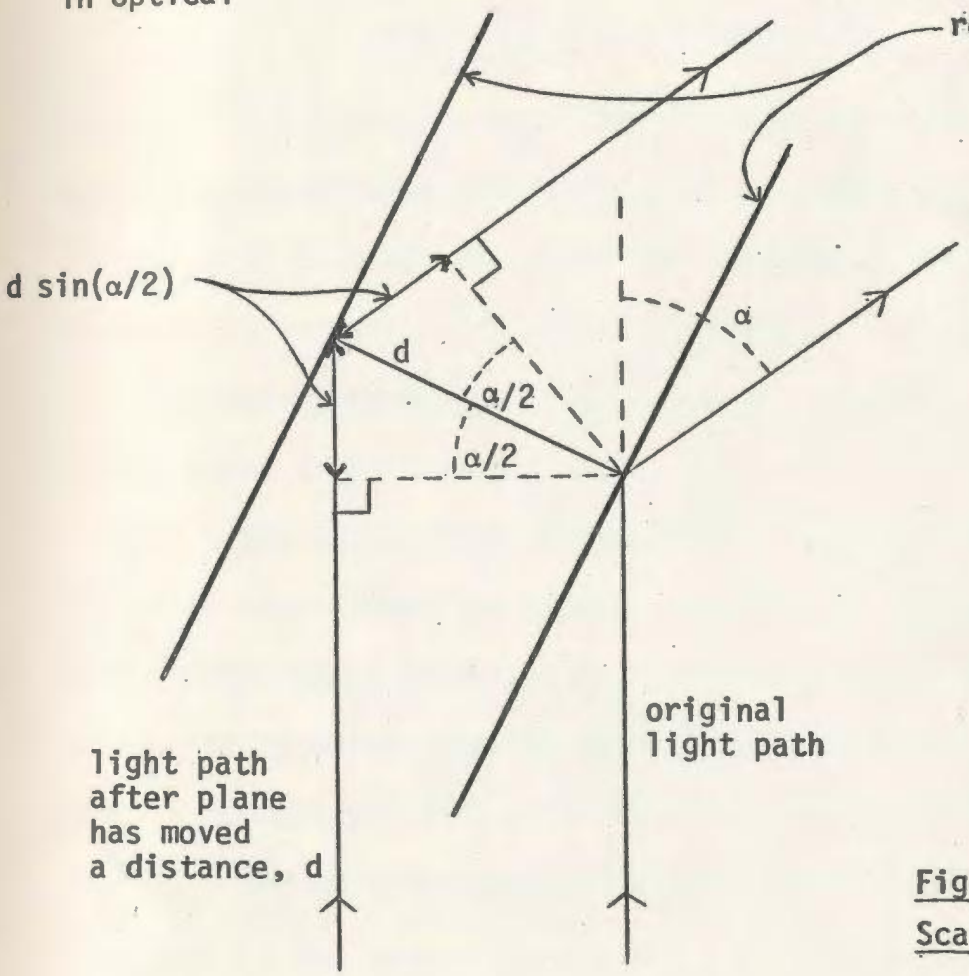

Figure 1 - Brillouin Scattering geometry

path is then 2 n d sin(α/2) where n is the mean refractive index of the crystal. Thus, a velocity, V, of the reflecting planes is equivalent to a velocity, 2 n V sin(α/2), of the light source. This apparent source velocity induces a Doppler shift (Jenkins and White, 1957),

$\Omega \equiv \nu_{observed} - \nu$, given by,

$$\Omega = \frac{\nu}{c} (2 n V \sin(\alpha/2)) \qquad 1\text{-}40$$

where ν is the frequency of the light incident on the experiment. Written in terms of the wavelength, λ of the incident light, equation 1-40 becomes:

$$\Omega = \frac{2 n V}{\lambda} \sin (\alpha/2) \qquad 1\text{-}41$$

The frequency shift, Ω, can be positive or negative depending on whether the direction of wave motion results in a decrease or increase in the optical path from the source to the observer. The elastic waves necessary to produce Brillouin scattering are found to arise spontaneously from random thermal excitations in a crystal and they thus propagate in arbitrary directions.

The combination of equations 1-41 and 1-39 enable the elastic constants of a single hexagonal crystal to be determined from frequency shifts observed in light scattering experiments. This procedure is particularly useful when the physical properties of a crystal are such that it is very delicate or difficult to grow and handle. This is the case with low melting point molecular crystals such as carbon monoxide.

CHAPTER 2

ORIENTATION OF SINGLE CRYSTALS

2.1 Introductory Remarks

This chapter describes a procedure for determining the orientation of a single crystal from data obtained using the Laue x-ray diffraction technique (for a discussion of some of the theoretical and practical aspects of the Laue technique see, for instance, Cullity, 1956 or Azaroff, 1968). The method can be applied to crystals from any system and the results, with the exception of two sets of transformation equations, are useable with either transmission or back reflection Laue data. To treat the back reflection case it is necessary to replace the transformation equations (equations 2-36 and 2-37) with those appropriate for back reflection geometry. Throughout the discussion it is assumed that the crystal orientation is arbitrary and initially unknown and that neither the crystal nor the x-ray source and camera is movable. Hence it is necessary to find the orientation without utilizing a particular advantageous alignment of the crystal and x-ray beam. The algebraic expressions involved in the orientation procedure are best evaluated using either a computer or a programmable calculator as without these aids the computations would be extremely unwieldy. If such a machine is used, however, the method can provide a reasonably fast and efficient means of obtaining a determination of crystal orientation.

2.2 Mathematical Preliminaries

Let $\hat{i}$, $\hat{j}$, $\hat{k}$ be unit vectors of a cartesian coordinate system

fixed in a single crystal and let $\vec{a}$, $\vec{b}$, $\vec{c}$ be the translation vectors defining a unit cell in the system to which the crystal belongs. In terms of the cartesian unit vectors the translation vectors can be written:

$$\vec{a} = q_{11}\,\hat{i} + q_{12}\,\hat{j} + q_{13}\,\hat{k}$$

$$\vec{b} = q_{21}\,\hat{i} + q_{22}\,\hat{j} + q_{23}\,\hat{k} \qquad 2\text{-}1$$

$$\vec{c} = q_{31}\,\hat{i} + q_{32}\,\hat{j} + q_{33}\,\hat{k}$$

Thus,

$$\begin{pmatrix} g_1 \\ g_2 \\ g_3 \end{pmatrix} = Q^{\dagger} \begin{pmatrix} G_1 \\ G_2 \\ G_3 \end{pmatrix} \qquad 2\text{-}2$$

where (g_1, g_2, g_3) are the cartesian components of a vector $\vec{G} \equiv G_1\,\vec{a} + G_2\,\vec{b} + G_3\,\vec{c}$ and $Q^{\dagger}$ is the transpose of the matrix Q defined by:

$$Q \equiv \begin{pmatrix} q_{11} & q_{12} & q_{13} \\ q_{21} & q_{22} & q_{23} \\ q_{31} & q_{32} & q_{33} \end{pmatrix} \qquad 2\text{-}3$$

An arbitrary plane displaced a distance S from the origin and perpendicular to a unit vector $\hat{n}$ consists of all vectors $\vec{G}$ satisfying:

$$\hat{n} \cdot \vec{G} = S \qquad 2\text{-}4$$

In matrix notation equation 2-4 can be written:

$$(n_1\ n_2\ n_3) \begin{pmatrix} g_1 \\ g_2 \\ g_3 \end{pmatrix} = S \qquad 2\text{-}5$$

where (n_1, n_2, n_3) and (g_1, g_2, g_3) are the cartesian components of $\hat{n}$ and $\vec{G}$ respectively.

Using equation 2-2 to express 2-5 with $\vec{G}$ written in terms of the unit cell basis vectors yields:

$$(n_1\ n_2\ n_3)\ Q^{\dagger} \begin{pmatrix} G_1 \\ G_2 \\ G_3 \end{pmatrix} = S \qquad 2\text{-}6$$

By definition (Kittel, 1976), a crystal plane with Miller indices, (h k l), is defined by the 3 vectors $\frac{\vec{a}}{h}$, $\frac{\vec{b}}{k}$ and $\frac{\vec{c}}{l}$.

Equation 2-6 is satisfied for each of these vectors yielding the three equations below:

$$(n_1\ n_2\ n_3)\ Q^{\dagger} \begin{pmatrix} 1 \\ 0 \\ 0 \end{pmatrix} = Sh; \quad (n_1\ n_2\ n_3)\ Q^{\dagger} \begin{pmatrix} 0 \\ 1 \\ 0 \end{pmatrix} = Sk;$$

$$(n_1\ n_2\ n_3)\ Q^{\dagger} \begin{pmatrix} 0 \\ 0 \\ 1 \end{pmatrix} = Sl \qquad 2\text{-}7$$

These can be combined to form the single matrix equation:

$$(n_1\ n_2\ n_3)\ Q^{\dagger} \begin{pmatrix} 1 & 0 & 0 \\ 0 & 1 & 0 \\ 0 & 0 & 1 \end{pmatrix} = (Sh\ Sk\ Sl) \qquad 2\text{-}8$$

This simplifies to:

$$(n_1\ n_2\ n_3)\ Q^{\dagger} = S(h\ k\ l) \qquad 2\text{-}9$$

Multiplying by $(Q^{\dagger})^{-1}$ and transposing both sides yields,

$$\begin{pmatrix} n_1 \\ n_2 \\ n_3 \end{pmatrix} = SQ^{-1} \begin{pmatrix} h \\ k \\ l \end{pmatrix} \qquad 2\text{-}10$$

where (n_1, n_2, n_3) are the direction cosines of the normal to the crystal plane with Miller indices (h k l) and S is the interplanar spacing for planes of the form {h k l}.

Let (x, y, z) be the direction cosines of the normal to a crystal plane expressed in a laboratory cartesian coordinate system. Assume that the laboratory system differs from the cartesian coordinate system fixed in the crystal by an arbitrary rotation. Then,

$$\begin{pmatrix} x \\ y \\ z \end{pmatrix} = R^{-1} \begin{pmatrix} n_1 \\ n_2 \\ n_3 \end{pmatrix} \qquad 2\text{-}11$$

where, $R \equiv \begin{pmatrix} r_{11} & r_{12} & r_{13} \\ r_{21} & r_{22} & r_{23} \\ r_{31} & r_{32} & r_{33} \end{pmatrix}$ is the rotation matrix

which transforms a vector expressed in the laboratory coordinates into the crystal coordinate system. Substituting equation 2-11 into equation 2-10 yields:

$$\begin{pmatrix} x \\ y \\ z \end{pmatrix} = SR^{-1} Q^{-1} \begin{pmatrix} h \\ k \\ l \end{pmatrix} \qquad 2\text{-}12$$

This is the fundamental equation for establishing the orientation of a single crystal using data obtained from Laue photographs. The unknown quantities in the equation are generally the rotation matrix R and the Miller indices (h k l) while the known quantities are the matrix Q specified by the crystal structure and the direction cosines (x, y, z) which can be calculated from the Laue data. The first step in solving the equation is to eliminate R. Using data for two crystal planes (denoted by subscripts 1 and 2) this can be done in the following manner. The transpose is taken of both sides of 2-12, to yield, in the case of plane 1:

$$(x, y, z) = S_1 (h_1 k_1 l_1) (Q^{-1})^{\dagger} R \qquad 2\text{-}13$$

Forming the product of the right and left sides of this equation with the right and left sides respectively of equation 2-12 gives:

$$(x_1\ y_1\ z_1)\begin{pmatrix} x_2 \\ y_2 \\ z_2 \end{pmatrix} = S_1\ S_2\ (h_1\ k_1\ l_1)(Q\ Q^{\dagger})^{-1}\begin{pmatrix} h_2 \\ k_2 \\ l_2 \end{pmatrix} \qquad 2\text{-}14$$

Each side of equation 2-14 is an expression for the scalar product between the normals to two crystal planes. Taking the two planes to be identical enables the interplanar spacing, S, corresponding to a given set of indices to be calculated from 2-14, as indicated below.

$$\frac{1}{S^2} = (h\ k\ l)\ (Q\ Q^{\dagger})^{-1}\begin{pmatrix} h \\ k \\ l \end{pmatrix} \qquad 2\text{-}15$$

Equation 2-14 alone can never uniquely specify the Miller indices of two crystal planes. Thus, data for at least three planes is necessary, although not always sufficient, to determine the indices. Equation 2-12 can be expressed for three planes simultaneously in the following manner,

$$A = R^{-1}\ Q^{-1}\ B \qquad 2\text{-}16$$

where $$A \equiv \begin{pmatrix} x_1 & x_2 & x_3 \\ y_1 & y_2 & y_3 \\ z_1 & z_2 & z_3 \end{pmatrix} \text{ and } B \equiv \begin{pmatrix} S_1 h_1 & S_2 h_2 & S_3 h_3 \\ S_1 k_1 & S_2 k_2 & S_3 k_3 \\ S_1 l_1 & S_2 l_2 & S_3 l_3 \end{pmatrix}$$

Taking the determinant of both sides of 2-16 gives the useful result,

$$|A| = \frac{S_1\ S_2\ S_3}{V}\begin{vmatrix} h_1 & h_2 & h_3 \\ k_1 & k_2 & k_3 \\ l_1 & l_2 & l_3 \end{vmatrix} \qquad 2\text{-}17$$

where $V \equiv |Q|$ is the volume of the unit cell. If each side of equation 2-17 is non-zero then the matrices A and B are invertable. Thus, from 2-16,

$$R = Q^{-1} B A^{-1} \qquad 2\text{-}18$$

For this equation to be valid two conditions are necessary and sufficient. Firstly, $|Q^{-1} B A^{-1}| = +1$, which gives rise again to equation 2-17. Secondly:

$$(A^{-1} B A^{-1})^{-1} = (Q^{-1} B A^{-1})^{\dagger} \qquad 2\text{-}19$$

$$\leftrightarrow \quad A^{\dagger} A = B^{\dagger} (Q Q^{\dagger})^{-1} B \qquad 2\text{-}20$$

Performing the multiplications in equation 2-20 yields,

$$\begin{pmatrix} 1 & D_{12} & D_{13} \\ D_{12} & 1 & D_{23} \\ D_{13} & D_{23} & 1 \end{pmatrix} = \begin{pmatrix} 1 & D'_{12} & D'_{13} \\ D'_{12} & 1 & D'_{23} \\ D'_{13} & D'_{23} & 1 \end{pmatrix} \qquad 2\text{-}21$$

Where D_{ij} is the dot product expressed on the left hand side of equation 2-14 for planes i and j and D'_{ij} is the corresponding expression on the right hand side of equation 2-14. Thus, if indices can be assigned to each of three independent crystal planes so as to satisfy the three interplanar dot product relations (equation 2-14) along with the determinant relation (equation 2-17) then a rotation matrix satisfying 2-12 for each of the three planes exists and is given by 2-18. In the above context, the word independent is taken to mean that the normals to the three planes are non-coplanar, or equivalently that the three planes do not lie in a single crystallographic zone. This condition is fulfilled when the determinant in equation 2-17 is non-zero.

At this point it should be noted that although equations 2-17

and 2-21 provide as good a check as is possible on the Miller index assignment for three planes, better reliability can be obtained by assigning indices to all planes observed on a Laue photograph and checking equation 2-14 for each pair. Furthermore, due to experimental error in determining the laboratory system direction cosines (x, y, z) for the various planes, a least squares fitting procedure, rather than equation 2-18, provides the best means of calculating the rotation matrix. One such procedure is discussed below.

2.3 Least Squares Rotation Matrix

Assume that Miller indices (h^i k^i l^i) have been assigned to each member (denoted by superscript i) of a set of not less than two crystal planes. It is then required to find the rotation matrix R which, through equation 2-12, best fits the experimental data. A squared error term, E, can be associated with a given trial rotation matrix as follows:

$$E = \sum_i \{(x^i_{exp} - x^i)^2 + (y^i_{exp} - y^i)^2 + (z^i_{exp} - z^i)^2\} \qquad 2\text{-}22$$

In the above expression $(x^i_{exp}, y^i_{exp}, z^i_{exp})$ are the laboratory system direction cosines of the normal to plane i as determined directly from the experimental data. The predicted direction cosine values (x^i, y^i, z^i) are found from equation 2-12 using the trial rotation matrix, R, along with the known Miller indices. Minimizing E, which provides a convenient criterion for specifying a "best fit" rotation matrix, is equivalent to maximizing the quantity F given below.

$$F = \sum_i (x^i_{exp}\ y^i_{exp}\ z^i_{exp}) \begin{pmatrix} x^i \\ y^i \\ z^i \end{pmatrix} \qquad 2\text{-}23$$

At this point it is useful to define the square matrix T to be,

$$T = \sum_i \begin{pmatrix} n^i_1 \\ n^i_2 \\ n^i_3 \end{pmatrix} (x^i_{exp}\ y^i_{exp}\ z^i_{exp}) \qquad 2\text{-}24$$

where (n^i_1, n^i_2, n^i_3) are the crystal system direction cosines for plane i as calculated from the Miller indices using equation 2-10. In terms of the elements t_{jk} of the matrix T defined above and the elements r_{jk} of the rotation matrix R defined as in equation 2-11, equation 2-23 becomes,

$$F = \sum_{j=1}^{3} \sum_{k=1}^{3} r_{jk}\ t_{jk} \qquad 2\text{-}25$$

or equivalently, $F = \text{trace}\ (RT^{\dagger})$.

Euler angles (ϕ, θ, ψ) (defined as in Goldstein, 1950) can be used to express R in terms of parameters which are independent.

$$R = \begin{pmatrix} \cos\psi\cos\phi - \cos\theta\sin\phi\sin\psi & \cos\psi\sin\phi + \cos\theta\cos\phi\sin\psi & \sin\psi\sin\theta \\ -\sin\psi\cos\phi - \cos\theta\sin\phi\cos\psi & -\sin\psi\sin\phi + \cos\theta\cos\phi\cos\psi & \cos\psi\sin\theta \\ \sin\theta\sin\phi & -\sin\theta\cos\phi & \cos\theta \end{pmatrix} \qquad 2\text{-}26$$

The following partial derivative equations are then necessary conditions for F to be a maximum.

$$\frac{\partial F}{\partial \phi} = 0, \quad \frac{\partial F}{\partial \theta} = 0, \quad \frac{\partial F}{\partial \psi} = 0 \qquad 2\text{-}27$$

Explicit evaluation of the derivatives, followed by replacement of the trigonometric expressions with appropriate rotation matrix elements, r_{jk},

can be used to find the following equations which are equivalent to 2-27.

$$\frac{\partial F}{\partial \phi} = 0 \leftrightarrow \sum_{j=1}^{3} r_{j1}\, t_{j2} - r_{j2}\, t_{j1} = 0$$

$$\frac{\partial F}{\partial \theta} = 0 \leftrightarrow \sum_{j=1}^{3} \sum_{k=1}^{3} r_{j3}\, r_{3k}\, t_{jk} = t_{33} \qquad 2\text{-}28$$

$$\frac{\partial F}{\partial \psi} = 0 \leftrightarrow \sum_{k=1}^{3} r_{1k}\, t_{2k} - r_{2k}\, t_{1k} = 0$$

The equations 2-28 can be derived from the combination of the matrix equation,

$$TR^{\dagger} = RT^{\dagger} \qquad 2\text{-}29$$

along with the rotation matrix property, $R^{\dagger} = R^{-1}$.

A convenient iteration procedure*can be used to find a solution to the above equation. Let $V^{(n)}$ denote the matrix obtained after performing n iteration steps defined as follows.

$$V^{(o)} = T, \qquad V^{(n)} = \frac{(V^{(n-1)} + \text{cof } V^{(n-1)})}{N^{(n-1)}} \qquad 2\text{-}30$$

where: cof V = matrix whose entries, $[\text{cof } V]_{jk}$, are cofactors of the entries $[V]_{jk}$, of the matrix V

and, $$N^{(n-1)} = [\sum_{k=1}^{3}([V^{(n-1)}]_{1k} + [\text{cof } V^{(n-1)}]_{1k})^2]^{\frac{1}{2}}$$

Assume that the sequence of matrices, $V^{(n)}$, specified by the above iteration converges and that each matrix in the sequence is invertable. It can then be shown that the limit matrix found in performing the iteration is a rotation matrix satisfying equation 2-29. Let m be the

*apparently not to be found in the literature

number of iteration steps needed to produce convergence to a given degree of accuracy. Then, to within the accuracy specified:

$$V^{(m)} = V^{(m-1)}$$

$$\rightarrow V^{(m)} = \frac{V^{(m)} + \text{cof } V^{(m)}}{N^{(m)}}$$

$$\rightarrow \frac{V^{(m)}}{N^{(m)}-1} = \text{cof}\left(\frac{V^{(m)}}{N^{(m)}-1}\right)$$

$$\rightarrow \frac{V^{(m)}}{N^{(m)}-1} \quad \text{is a rotation matrix} \qquad 2\text{-}31$$

Condition 2-31 implies that the sum of the squares of the entries in the top row of the matrix, $V^{(m)}/(N^{(m)}-1)$ is 1. The definition of $N^{(m)}$ makes the same relation hold for the top row of $V^{(m)}$. Thus,

$$\frac{1}{(N^{(m)}-1)^2} = 1$$

$$\rightarrow N^{(m)} = 2$$

Therefore, by 2-31, $V^{(m)}$ is a rotation matrix.

The equations,

$$T(V^{(n)})\dagger = V^{(n)}\, T\dagger \qquad 2\text{-}32$$

and,

$$(V^{(n)})\dagger\, T = T\dagger\, V^{(n)} \qquad 2\text{-}33$$

are both trivially satisfied when n=0. Using the identity,

$$\text{cof } V^{(n)} = |V^{(n)}|\ [(V^{(n)})^{-1}]\dagger$$

it can be seen that if equations 2-32 and 2-33 hold for $V^{(n)}$ then they

must also hold for $V^{(n+1)}$. Thus, by induction, these equations are satisfied by the matrix, $V^{(n)}$, obtained in each iteration step and hence by the limit matrix $V^{(m)}$. Therefore, setting $R = V^{(m)}$ yields a solution to equation 2-29.

Although equation 2-29 expresses the necessary conditions on R in order that the squared error E be a minimum, it is not sufficient to eliminate other possible critical points of the function $E(\phi, \theta, \psi)$ at which an absolute minimum does not occur. It can however be conjectured on the basis of extensive numerical evidence that the matrix, R, found using the iteration procedure indicated above, minimizes E and can thus be taken to be the "least squares" rotation matrix.

2.4 Orientation Procedure

As a first step in determining the orientation of a single crystal from transmission Laue data it is necessary to define cartesian coordinate systems in both the laboratory and crystal frames of reference. A convenient way to specify the laboratory coordinates is to use the plane of the Laue photograph and the path of the undeflected x-ray beam to define the axes. Throughout the following discussion, the x axis in the laboratory system is taken to be a horizontal axis parallel to the plane of the Laue photograph. The y axis is defined such that the undeflected x-ray beam travels along the y axis in the positive direction. A unit vector $\hat{k}$, in the z direction is then defined by $\hat{k} = \hat{i} \times \hat{j}$ where $\hat{i}$ and $\hat{j}$ are unit vectors in the x and y directions respectively. The origin of the laboratory coordinate system lies inside the crystal at a distance D from the surface of the Laue photograph. Points on the

photograph thus have coordinates of the form (x, D, z). To simplify notation, these will henceforth be referred to as (x', z'). The set of axes described above is illustrated in figure 2.

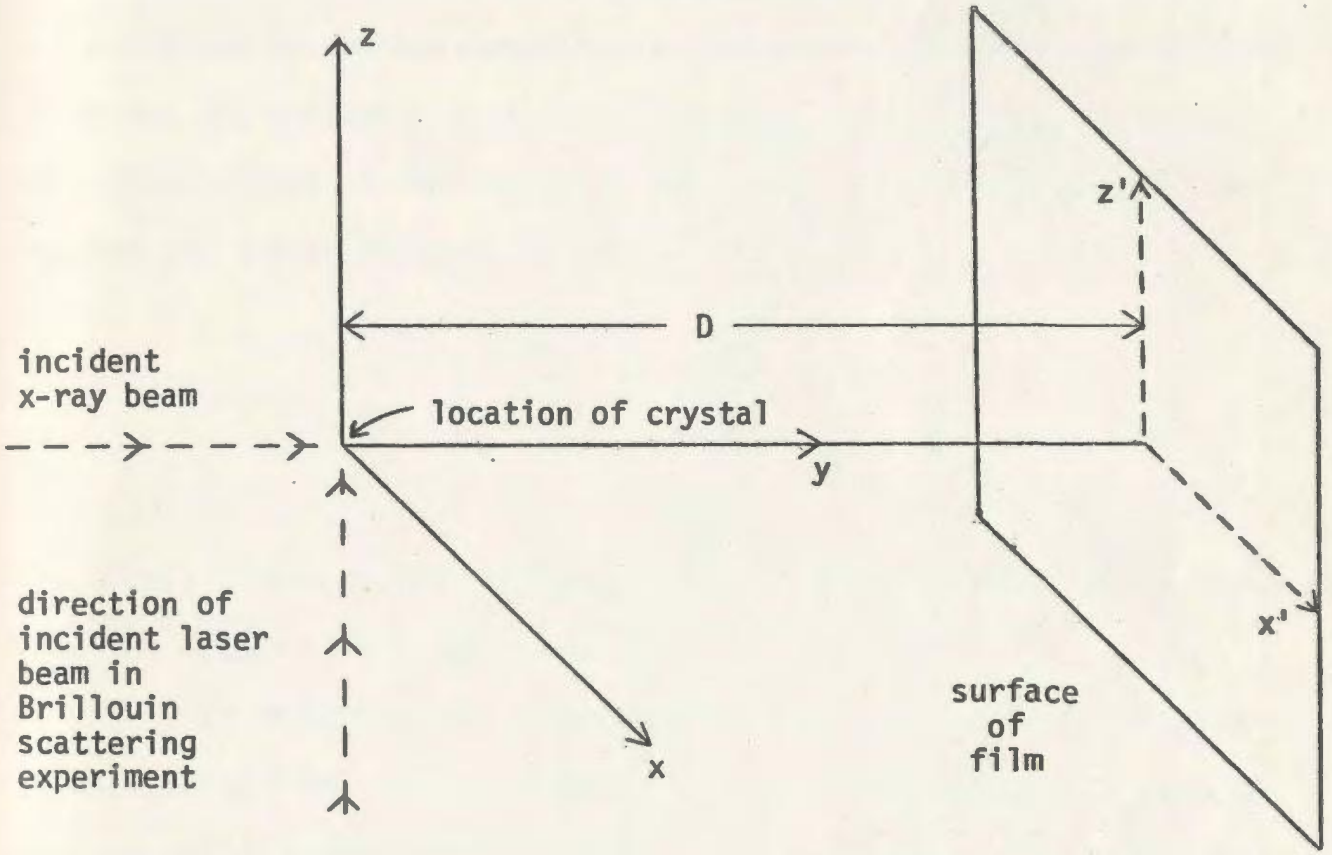

Figure 2 - Laboratory coordinate system

The best choice for the coordinate system fixed in the crystal is that which most simplifies the matrix Q defined in equation 2-3. Usually this means having the axes lie along the translation vectors defining the unit cell wherever possible. For example, if a crystal has

cubic symmetry,

$$Q = \begin{pmatrix} a & 0 & 0 \\ 0 & a & 0 \\ 0 & 0 & a \end{pmatrix} \qquad 2\text{-}34$$

represents the most convenient choice of crystal frame axes, whereas for a crystal in the hexagonal system, a good way of defining the axes is to use the crystal c axis to define the z direction and have the y direction be that of the crystal b axis. The hexagonal geometry then implies the following form for Q:

$$Q = \begin{pmatrix} \frac{a\sqrt{3}}{2} & -\frac{a}{2} & 0 \\ 0 & a & 0 \\ 0 & 0 & c \end{pmatrix} \qquad 2\text{-}35$$

The origin of the crystal frame coordinate system is taken to be coincident with the origin of the lab system.

To determine the lab frame direction cosines, (x, y, z), of a crystal plane from the coordinates, (x', z'), of its Laue diffraction spot, a set of transformation equations is necessary. The only aspect of the theory of x-ray diffraction required in obtaining the equations is the geometrical result that x-rays appear to experience mirror-like reflection from the crystal planes. That is, the incident and reflected beams are coplanar with the normal to the reflecting plane, and the angle of incidence equals the angle of reflection. Using this result, along with the geometry indicated in figure 2, the transformation equations are found to be:

$$x = \frac{x'}{r\sqrt{2}} \left(1 + \frac{D}{\sqrt{r^2 + D^2}} \right)^{\frac{1}{2}}$$

$$y = -\frac{1}{\sqrt{2}} \left(1 - \frac{D}{\sqrt{r^2 + D^2}} \right)^{\frac{1}{2}} \qquad 2\text{-}36$$

$$z = \frac{z'}{r\sqrt{2}} \left(1 + \frac{D}{\sqrt{r^2 + D^2}} \right)^{\frac{1}{2}}$$

where $r = \sqrt{x'^2 + z'^2}$.

The inverse transformation is given by:

$$x' = x \left(\frac{2\, y\, D}{2\, y^2 - 1} \right) \qquad 2\text{-}37$$

$$z' = z \left(\frac{2\, y\, D}{2\, y^2 - 1} \right)$$

Once the lab frame direction cosines of the normals to the crystal planes represented on a Laue photograph have been calculated, Miller indices can be assigned. The procedure for choosing the indices invariably involves some sort of trial and error routine, rather than an explicit computation. This results from the fact that no amount of experimental data will specify a unique solution to equation 2-12. The equation can be solved only by assuming that the possible sets of Miller indices which can be assigned to the observed planes must be drawn from a finite list. This list is generally determined by the composition and

crystal structure of a given sample.

Equation 2-17 can be used as a convenient first step in finding the indices of three planes which do not lie in the same zone. This is done by calculating $|A|$ and then substituting various values of the plane spacings S_1, S_2 and S_3 into the equation until a potentially valid set of spacings is found. Since,

$$\begin{vmatrix} h_1 & k_1 & l_1 \\ h_2 & k_2 & l_2 \\ h_3 & k_3 & l_3 \end{vmatrix}$$

must be an integer, a large number of possible sets of spacings can be eliminated without necessarily knowing the actual value of this determinant. The magnitude of the interplanar spacing indicates the form to which a crystal plane belongs. In general, planes of a given form are related by symmetry and have equal spacings and identical x-ray diffraction properties. In this discussion though, the word form will be used to denote any set of planes with identical spacings. In many cases the two definitions will yield equivalent results. However, in cases where the crystal class being considered is not the one having the highest symmetry for the appropriate system, there may be planes with equal spacings which are not symmetrically equivalent, and thus, in terms of the standard definition, not in the same form.

The possible sets of Miller indices which can be assigned to a plane of a given form are determined by equation 2-15. A simple rule, resulting from the spacing equation, can generally be applied. For instance, in the case of a cubic crystal:

$$S = \frac{a}{\sqrt{h^2 + k^2 + l^2}}$$

Thus all, (a maximum of 48), planes of the form {h k l} can be found by permuting or changing the signs of h, k and l since these are the operations which leave S unchanged. In the hexagonal case the spacing equation is,

$$S = \frac{a\sqrt{3}}{2\sqrt{h^2 + hk + k^2 + \frac{3}{4}\left(\frac{a}{c}\right)^2 l^2}}$$

and planes of the form {h k i l}, (using Miller-Bravais indices, -i = h + k), are found by permuting h, k and i, or changing the sign of l or simultaneously changing the signs of h, k and i.

The dot product relation, equation 2-14 can be used not only in determining the exact indices for a set of crystal planes but also, as a preliminary step, for determining the appropriate forms. This procedure requires a table listing pairs of form indices, $\{h_1\ k_1\ l_1\}$ - $\{h_2\ k_2\ l_2\}$, versus the possible dot products (or equivalently, interplanar angles) between the normals to planes in the respective forms. Correlating tabulated with observed values of the dot product then enables form indices to be assigned to the various planes with substantially less ambiguity than is possible using only the determinant relation. Assigning an exact set of indices to each of at least three planes is the final step required before a tentative rotation matrix can be calculated. The assignment is done by trial and error, using as a test, the three dot products and the determinant relation indicated in the mathematical preliminaries. The procedure can often be simplified

greatly if the forms to which the three planes belong have been determined in advance. Once correct Miller indices have been assigned to any two or more planes, a rotation matrix can be found using the least squares procedure described previously.

After using the method discussed above to determine a preliminary rotation matrix it is then possible to explicitly calculate the indices of all planes for which lab frame direction cosines are known. Usually, due to experimental error, indices calculated using a rotation matrix are not exact integers and hence must be rounded off. The procedure can provide a reliable check and, as well, a means of rapidly indexing additional planes represented on a Laue photograph which have not already been indexed using the trial and error method. After having determined indices for all experimentally observed planes, the complete set of data can be used to calculate a final "least squares" rotation matrix. Euler angles corresponding to this matrix can be found using the general expression for the rotation matrix as a function of the Euler angles which is given in equation 2-26.

CHAPTER 3

EXPERIMENTAL SETUP AND PROCEDURE

3.1 Growth of Single Crystals of β-Carbon Monoxide

In order to use Brillouin spectroscopy to determine the elastic constants of a crystalline substance it is first necessary to be able to produce good quality single crystals of that substance. Good quality refers both to the optical properties and to the internal structure of the crystal. The important optical properties are that the crystal be transparent and free from mechanical imperfections such as cracks, bubbles or imbedded particles of impurities. The internal structure of the crystal must be such that an x-ray diffraction pattern reveals that the crystal is completely single and is not deformed.

To grow a crystal of carbon monoxide having the properties mentioned above requires careful control of temperatures, cooling rates and thermal gradients within the sample. The cryogenic apparatus required for this purpose was designed to handle a variety of molecular gases and had already been used in experiments on solid oxygen (Kiefte and Clouter, 1975) and nitrogen (Kiefte and Clouter, 1976) prior to beginning the experiment on CO. Details of its construction are given in the above (oxygen) reference and hence will only be outlined here. For convenience a diagram of the cryostat tail section and sample cell is reproduced in figure 3. The bracketed capital letters in the following paragraph refer to this figure.

The cell (N) in which the carbon monoxide crystals were grown

Figure 3* - Cryostat Tail Section and Sample Cell

A	stainless steel outer jacket
B	radiation shield
C	liquid-helium tube
D	helium gas exhaust
E	Teflon spacer
F	radiation shield
G	heater
H	stainless steel sample tube
I	threaded brass heat sink
J	flexible copper braid
K	large plexiglass window
L	aluminum foil
M	heaters
N	cell
O	spring clamp
P	quartz plug
Q	quartz window

* reproduced from paper by Kiefte and Clouter (1975)

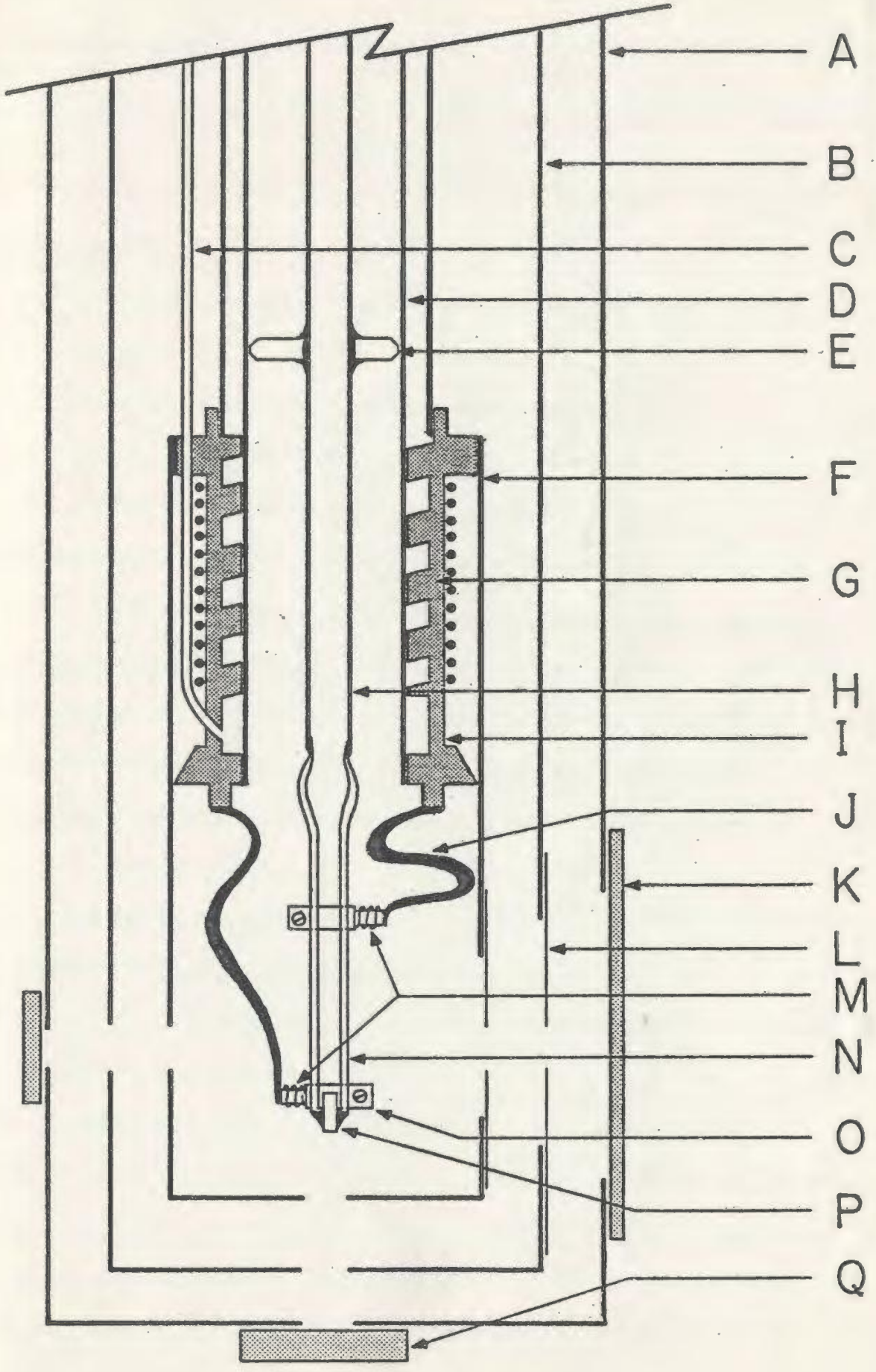

Figure 3

consisted of a quartz tube 2 cm long with an inside diameter of .3 cm and terminated by a quartz plug (P). Heat was removed from the cell via two copper braids (J), one connected to the cell bottom and one connected to the top. The braids were in turn soldered to a brass heat exchanger (I), which was cooled by allowing a controlled flow of vaporized liquid helium to circulate through it. The temperature of the heat exchanger was regulated using a GaAs thermal sensor and a heater (G), coupled through an appropriate feedback circuit. In addition, heaters (M) were mounted on the two clips (O), used to attach the copper braids to the cell and the temperature at the bottom clip was monitored with a GaAs detector. This detector provided the input to a second feedback circuit which was used in making fine adjustments to the cell temperature and controlling it to within .1 K. The thermal gradient in the cell was monitored using a copper - constantan differential thermocouple and could be controlled by a potentiometer which regulated the fraction of the total cell heater current supplied to either the top or bottom heater.

The first step in forming a crystal of carbon monoxide was to cool a sample of 99.99% pure CO (obtained from the Matheson Company) until a column of liquid filled the cell. The gas handling system was sealed off prior to cooling and thus, as cooling proceeded, the pressure above the cell dropped from near one atmosphere to the vapor pressure of liquid CO. A fairly elaborate sequence of steps was then used to grow a single crystal of the solid from the liquid. The preliminary step was to maximize the fraction of the cell heater current supplied to the top heater, thus maximizing the thermal gradient in the cell. The

temperature at the bottom of the cell was set 2.6 degrees above the triple point of CO (68.1 K) while the temperature of the heat exchanger was adjusted to 65.5 K. This difference in temperature between the heat exchanger and the cell bottom was, in fact, the maximum consistent with reliable control of the cell temperature.

Two empirical observations necessitated the pre-cooling procedure. Firstly, it was found that very rapid cooling through the freezing point was required in growing useable crystals and secondly, a high temperature gradient in the cell was needed to keep the initially formed "seed" crystal from growing more than 1 mm high. The rapid cooling was accomplished by abruptly turning the cell temperature controller down to 67.6 K and simultaneously resetting the heat exchanger temperature at 63.1 K. Since the initial temperature settings were such that the heat exchanger was substantially colder than the cell, heat was transferred very rapidly through the copper braids and the cell cooled to the desired temperature in less than one minute.

After reaching the triple point, a small column (approximately 1 mm) of frozen carbon monoxide appeared at the bottom of the cell. Although optically clear, the frozen sample was almost invariably found to be polycrystalline when checked by x-ray diffraction (see following section). It could, however, usually be converted to a single crystal by allowing it to anneal for a few hours (less than four in most cases). Since the annealing process occurred most rapidly very near the triple point, the cell temperature was increased to 68.0 K before beginning to anneal the sample. The warming was done gradually over a period of fifteen minutes. During this time the cell temperature gradient

was continuously reduced so as to keep the frozen sample from becoming so small that it could not be examined with the x-rays.

When a Laue diffraction pattern revealed that a single crystal seed with well defined planes had been formed, the final stage of cooling was started. With the aid of a clock drive mechanism connected to the potentiometer on the cell temperature controller, the temperature of the cell was reduced by about 0.1 degrees per hour for eight hours. The fraction of the cell heater current supplied to the upper and lower heaters was not altered during the cooling process. At the conclusion of cooling, the voltage on the differential thermocouple showed a temperature difference of 2.1 K between the top and bottom of the cell. Assuming linearity (not a particularly well justified assumption but the only one possible under the circumstances) this corresponded to a thermal gradient of 1.1 degrees per centimeter. The fully grown crystal was of the order of 1 cm high and had a temperature at the bottom of 67.1 K. The temperature at the midpoint (where the observable Brillouin scattering occurred) was estimated from the gradient to be $67.6 \pm .2$ K, 0.5 K below the triple point. A Laue photograph, taken at the conclusion of growth, was used to ensure that the crystal was single and free from flaws. The optical quality of the crystal could be tested with the beam from the argon ion laser used in the Brillouin scattering experiments.

The crystal growth procedure discussed above was evolved primarily by trial and error with the intention of maximizing the chances of growing a usable crystal on a given attempt. It was found that the above procedure yielded about one good crystal for every two attempts.

This represented a marked improvement over initial efforts where the general lack of reliability was best demonstrated by a sequence of twelve consecutive growth attempts without a single success.

3.2 Orientation of β-Carbon Monoxide Crystals

The orientation of a single crystal must be known before data obtained in a Brillouin scattering experiment can be used in determining elastic constants. In the case of β-carbon monoxide, which crystallizes in the hexagonal system, a knowledge of the crystal orientation is required in calculating the angle γ which appears in equation 1-39. This angle is necessary in linking experimentally observed frequency shifts with the elastic constants of CO.

In this experiment, the transmission Laue x-ray diffraction technique was used to establish the orientations of carbon monoxide crystals. The orientations were specified in a laboratory coordinate system defined with respect to an x-ray diffraction setup (see figure 2, chapter 2). The x-ray beam and camera were precisely aligned with the optical system used in observing Brillouin scattering, thus allowing accurate determination of γ from the crystal orientations indicated by the diffraction patterns. The x-ray setup consisted of a Philips MG100 x-ray source (operated at 70 KV, 10 mA) along with a lead collimator (9 cm long, .1 cm in diameter) and a Polaroid model XR-7 land camera using type 57 Polaroid film. The distance from the end of the collimator to the crystal was 7 cm while the distance from the crystal to the film surface was set at 7 cm for the first two crystals and at 8 cm for all subsequent crystals in the experiment. The collimator was aligned so as to transmit a helium-neon laser

beam which was used to define the optic axis (see following section). The camera was set perpendicular to this beam by mounting a mirror in the camera holder and then aligning the assembly so as to make the beam reflect precisely back on itself. Exposure times of the order of five minutes were used in making the Laue photographs.

As mentioned in the previous section, x-ray diffraction photographs were used not only for crystal orientation, but also for determining whether or not a sample of frozen CO was a useable single crystal. The quality of a crystal could usually be determined by visually inspecting a Laue photograph. A good single crystal was indicated if the Laue pattern showed well defined spots arranged so as to imply that the corresponding crystal planes occupied three or less crystallographic zones (see section 2, chapter 2). The presence of more than three zones was taken to indicate that the sample was polycrystalline. Zones were readily recognized by the fact that each spot in a zone, along with the spot produced by the undeflected x-ray beam lay along some conic section (ellipse, parabola, etc.).(Cullity, 1956). Another indication of a polycrystalline sample was the appearance of two spots lying very close together. It was assumed that, in most cases, spots from a single crystal would be separated by at least a few millimeters since all low order planes in a crystal of β-CO have an angular separation of at least 4.7^{o}. A flawed crystal was indicated if it yielded a Laue photograph with spots which were neither round nor elliptical. These shapes were the only ones which could result from diffraction by well formed crystal planes given that the incident x-ray beam had a round cross-section and a small but non zero divergence

(Cullity, 1956). Spots which were fuzzy and had arbitrary shapes were assumed to occur as a consequence of major faults in the internal structure of the crystal. Thus, crystals showing poorly defined spots were not used in the Brillouin scattering experiments.

When a Laue photograph implied that a crystal was single and of suitable quality, the procedure described below was used to determine its orientation. In almost all cases, crystals were oriented before attempting to obtain any Brillouin spectra from them. There were two reasons for this. Firstly, a consistent set of results from the orientation procedure guaranteed that the crystal was single. Secondly, knowledge of the orientation in advance of running the Brillouin spectra enabled specific values of γ (see section 3, chapter 1) to be chosen with the aim of having the experimental data represent the widest possible range of values of this parameter. The cell in which the crystals were grown had one rotational degree of freedom (rotation over a 120^{o} range about the laboratory z axis) which allowed most crystals to yield data at several different values of γ.

The first step in the orientation procedure involved measuring the coordinates, x' and z' (see section 4, chapter 2) of all spots on a Laue photograph. Originally, this was done using a comparator but later it was found that using a finely ruled rectangular grid provided a sufficiently accurate and much more rapid means of locating the spots. A grid with dimensions 8.3 cm by 5.5 cm ruled with 39.05 divisions/cm was photographically produced for this purpose.

Following determination of x' and z', the direction cosines, (x,y,z), of the various crystal planes were calculated using the trans-

transformation equations 2-36. As well, values of 4δ, ($\delta \equiv$ interplanar angle, $\cos \delta = (x_1x_2 + y_1 y_2 + z_1 z_2)$) were calculated for each pair of planes. These calculations, along with all others involved in the orientation procedure were performed using programs written for a Texas Instruments SR - 52 card programmable calculator.

Miller indices were subsequently assigned to the various planes using a two step procedure. In the first stage, only the forms (see section 4, chapter 2) of the planes were determined. These were found by correlating (to within $\pm 4^o$) all experimental values of 4δ with tabulated values corresponding to pairs of forms in hexagonal close-packed crystals. The necessary tables were constructed using the formula specified by the right hand side of equation 2-14 and are given in the appendix. The tables assume a value of the hexagonal axial ratio, c/a, which corresponds to an ideal hcp structure, that is $c/a = \sqrt{8/3} \simeq 1.63$. For CO, the ratio is found to be c/a = 1.65 (calculated from values of a and c given by Barrett and Meyer, 1965). The 1.2% discrepency was overlooked for the sake of generality when constructing the tables.

The matrix Q (see equations 2-3 and 2-35), which was utilized throughout the orientation procedure, was taken to be:

$$Q = \begin{pmatrix} 1 & -\frac{1}{\sqrt{3}} & 0 \\ 0 & \frac{2}{\sqrt{3}} & 0 \\ 0 & 0 & \frac{4\sqrt{2}}{3} \end{pmatrix} \qquad 3\text{-}1$$

This corresponded to the same axis choice used in writing the matrix 2-35,

along with values for a and c of $\frac{2}{\sqrt{3}}$ and $\frac{2}{\sqrt{3}} \cdot (\frac{\sqrt{8}}{3}) = \frac{4\sqrt{2}}{3}$ respectively. Having chosen the crystal system axes in this way was equivalent to specifying that the x axis be perpendicular to the plane with Miller indices (1 0 0), that the y axis be perpendicular to $(\bar{1}\ 2\ 0)$ and that the z axis be perpendicular to (0 0 1). The effect of the small error included in the c/a ratio was not determined, but the self consistency of the results observed when performing the orientations indicated that it was not significant.

The next stage in the indexing procedure was the assignment of explicit Miller indices to three crystal planes not lying in the same zone. This was accomplished using a sequence of four SR - 52 programs. The input data consisted of the forms to which the three planes belonged along with their experimentally determined direction cosines. The effect of the program was to assign trial sets of Miller indices to the three planes and then output the first combination of sets which were found to satisfy the determinant equation, 2-17, and the three interplanar dot product equations of the form 2-14. The trial Miller indices were derived from the appropriate form indices according to the rule dictated by the plane spacing equation for the hexagonal system (discussed in section 4, chapter 2).

Having established explicit Miller indices for three planes enabled a preliminary laboratory - to - crystal - frame rotation matrix to be calculated. This was done using the least squares procedure discussed in section 3, chapter 2. Firstly the matrix T defined in equation 2-24 was evaluated with the aid of an SR - 52 program. A subsequent program then

converted T into a least squares rotation matrix using the iteration procedure 2-30. As a final step, Euler angles corresponding to this matrix (as in equation 2-26) were calculated. These Euler angles could be thought of as implying an ordered (z axis, x' axis, z'' axis) sequence of rotations and were found useful primarily because the first rotation, ϕ, was about an axis coincident with the rotation axis of the cell in the cryostat.

To calculate the final version of the rotation matrix, incorporating all data present on the Laue photograph, it was first necessary to index the planes not already indexed in the above preliminary procedure. This was done by using the inverse of equation 2-12, along with the preliminary values for the Euler angles, to determine approximate indices for each plane directly from its direction cosines. Proper Miller indices were then found by rounding off the approximate indices. The procedure was carried out for all planes, including the three which had previously been indexed. Obtaining an acceptable set of approximate Miller indices (deviating from an integer by not more than .05) for every plane provided as reliable a check as was possible on the validity of the assumed rotation matrix. This method of direct indexing could be used any time an approximate set of Euler angles was known. In particular, it was useful in treating Laue photographs corresponding to arbitrary rotations of the crystal about the axis in the cryostat. Once an orientation has been determined for a given angle setting, the crystal could readily be reoriented when rotated to any other angle. The procedure for calculating a least squares rotation matrix from a set of indexed planes is identical regardless of the number of planes involved (this number must, of course,

be ≥ 2). Thus, the method used for the three planes in the preliminary orientation could always be applied.

In the course of performing the thirty-five crystal orientations used in this experiment, planes belonging to 12 different forms were observed. Listed approximately according to their relative frequency of appearance these were, {1 0 0}, {1 1 0}, {1 0 1}, {1 0 2}, {1 0 3}, {2 0 1}, {3 0 1}, {1 1 2}, {0 0 1}, {1 2 0}, {1 1 1}, {2 2 1}. The most intense spots were reflected from the {0 0 1}, {1 0 1}, and {1 0 0} forms. Reflections from planes of the forms {1 1 1} and {2 2 1} were extremely faint and were only observed twice and once respectively. No attempt was made to justify the presence, or absence, or the observed brightnesses of spots due to planes of the various forms. However, it could be noted that the combination of the minimum x-ray wavelength (λ_{min} = .177 Å) and the crystal lattice parameters (α = 6.85 Å, C = 4.14 Å) was such that cutoff resulting from the Bragg condition, $\lambda_{min} = 2S \sin(\theta_{min})$, did not likely represent a significant factor.

3.3 The Optical System

Five primary components made up the optical system utilized in obtaining the Brillouin spectrum of CO. An argon ion laser provided a highly monochromatic light source for the experiment. A quartz sample cell and associated optics were used in guiding the laser beam through a crystal of CO and observing the light scattered at 90°. The scattered light was resolved into its frequency components with a Fabry-Perot interferometer. A photomultiplier and associated optics detected the

scattered light while an electronic unit (Data Aquisition and Stabilization system ≡ DAS) controlled the interferometer and collected the data output by the photomultiplier. A diagram of the experimental setup, illustrating the geometry of the optical system, appears in figure 4.

The argon ion laser (Spectra Physics model 165-08), which was used in this experiment featured very high stability and narrow linewidth in its output frequency. A prism in the laser cavity was angled so as to limit laser action to the 5145 Å line in the Ar^+ spectrum. Dispersion by the prism caused all other lines to be deviated so as to strike the rear laser mirror at non-normal incidence and hence not be returned to the cavity. Selection of a single axial mode (frequency satisfying condition for constructive interference in the laser cavity) from the Doppler broadened (width ≈5 GHz) Ar^+ spectral line was accomplished using a highly stable intracavity Fabry-Perot etalon. Adjacent transmission maxima of the etalon differed in frequency by more than the width of the Ar^+ line. Thus the etalon behaved as though it had just one peak transmission frequency and laser action was restricted to the axial mode lying nearest this peak. The effective linewidth of the laser output was of the order of .005 GHz (due mainly to "jitter" in the line frequency), too small to be resolved by the Fabry-Perot system used in analyzing the scattered light in this experiment. When the laser was warming up just after being turned on, mode hops (shifts in the particular axial mode passed by the intracavity etalon) were observed to result from thermally induced changes in the laser cavity length (or possibly in the spacing in the etalon). These, however, generally vanished after a half hour warmup period.

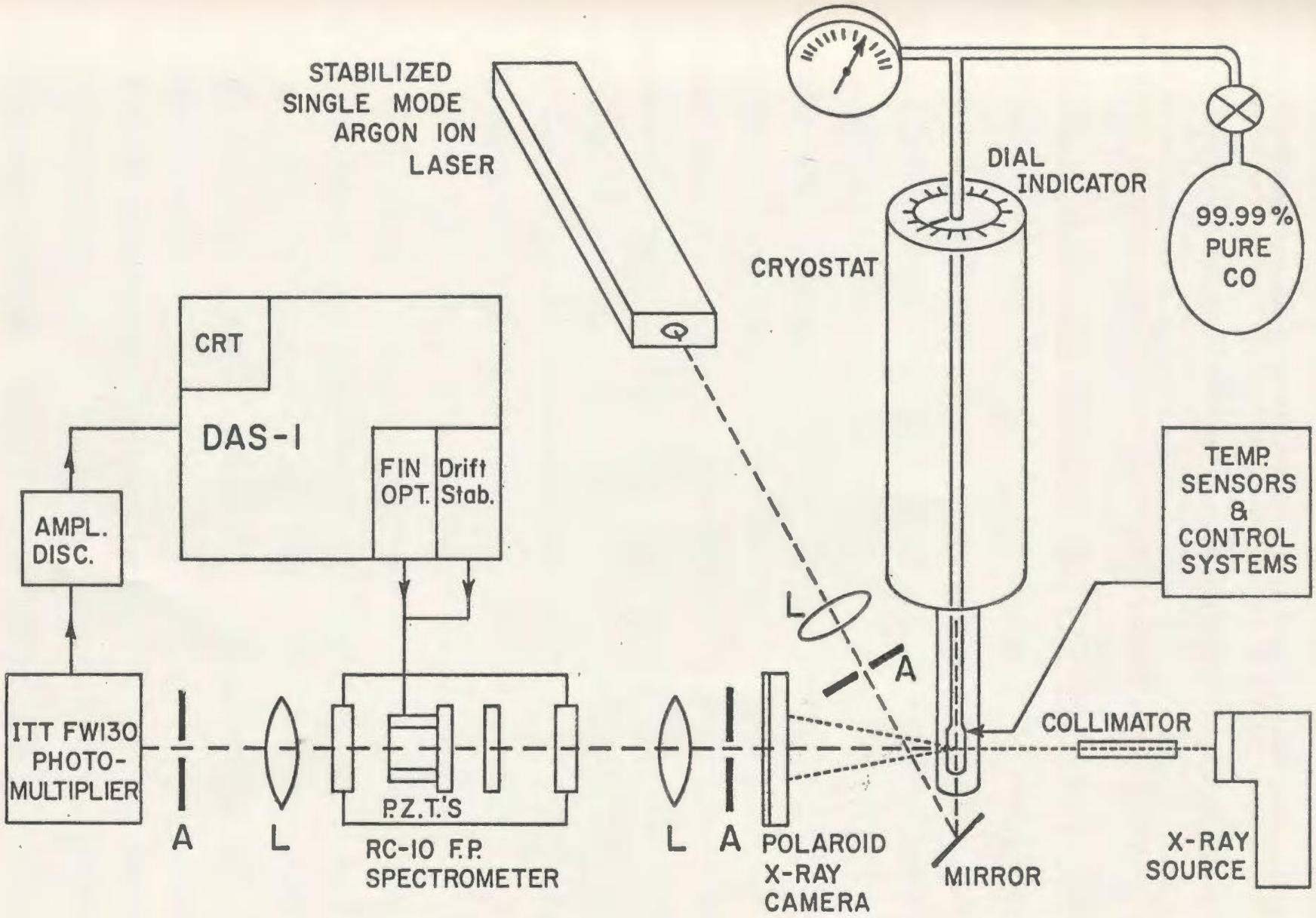

Figure 4 - Block diagram of experimental setup

The beam from the laser was directed by way of a beam steerer, a lens, an aperture and a mirror into the quartz cell containing the carbon monoxide crystal. The beam steerer was used both to reflect the beam through 90^{o}, and for preliminary positioning of the beam. The lens (focal length = 25.4 cm) was located so as to focus the laser light near the bottom of the quartz cell. This was advantageous since having the light pass through a very small area on the cell bottom minimized the odds of striking one of the dust particles which had inadvertently settled there. Foreign particles in the path of the laser beam caused drastic increases (often by a factor of 100 or more) in the amount of light scattered from the cell. This sometimes blotted out spectral features lying near in frequency to the unshifted laser line and in a few cases also resulted in overloading of the photomultiplier tube. As well, dust particles were a primary factor in the destruction of carbon monoxide crystals. This was due to their ability to absorb enough laser light to cause local melting and hence the formation of bubbles of liquid and cracks in a crystal.

The lens used to focus the laser beam also enabled fine adjustments to be made in the beam position. For this purpose the lens was held in an x-y mount and was adjusted so as to direct the beam through a point near the centre of the cell but away from any dust particles on the bottom. It was particularly important to centre the beam in the x direction (coordinates as in figure 2) in order to minimize changes in direction of the scattered light upon leaving the cell. An aperture located between the lens and the cell served as a rough spatial filter, removing stray light from the edge of the beam so as to reduce unwanted scattering. A mirror positioned under the bottom window of the cryostat

deflected the beam through 90^{o}. This made the beam direction parallel to the axis of the cell.

Since the scattering angle α (see section 3, chapter 1) was an important parameter in relating frequency shifts to elastic constants, it was necessary to insure that this angle was well defined by the geometry of the optical setup. To simplify alignment procedures, α was chosen to be 90^{o}. This was equivalent to specifying that the optic axis of the detection system be normal to the direction of the laser beam in the cell. A beam from a He - Ne laser (mounted securely in a stack of concrete blocks) was used to define the optic axis. Pinholes located at each end of a two meter optical bench guaranteed that only the light traveling along the axis could reach the photomultiplier tube. The angle α was set at 90^{o} by holding a pentaprism at the point where the vertical argon ion beam and the horizontal He - Ne beam intersected. Since the pentaprism reflected light through exactly 90^{o}, it was necessary only to make fine adjustments in the argon beam direction until the beam reflected from the pentaprism was parallel to the beam from the He - Ne laser.

Both a pinhole and a lens were located along the optic axis between the cell and the Fabry-Perot interferometer. The pinhole, .5 cm in diameter and 31 cm from the cell, limited the light reaching the interferometer to that scattered within a cone of angular radius $.5^{o}$. The lens (focal length = 40 cm) was positioned so as to have the beam in the cell at its focal point, thus insuring that the rays of scattered light reaching the interferometer were parallel. An x-y mount allowed the lens to be used in making fine adjustments to the path of light rays traveling from the pinhole to the interferometer. These adjustments had the effect of

changing the point in the cell which was "seen" by the light detection system. The lens could thus be aligned to make this point lie along the path of the laser beam in the crystal. Proper alignment was best indicated by the appearance of clearly observable Brillouin components in the spectrum of the scattered light.

Analysis of the scattered light was accomplished using a Burleigh, model RC-10 Fabry-Perot interferometer. The general theory of such a device is outlined in numerous optics texts, for example, Born and Wolf (1964) or Jenkins and White (1957). In addition, a more specific discussion can be found in the technical manual (No. FP 140 475, Tech Memo for Fabry-Perot Interferometry) for the Burleigh line of Fabry-Perots. The model RC-10 Fabry-Perot had a number of special features which made it particularly well adapted for resolving the Brillouin spectrum of CO. These included very high thermal stability, piezoelectric drives enabling remote control, high spectral resolution and a "triple pass" option to enhance contrast.

High thermal stability refers to the ability of a Fabry-Perot to resist thermally induced changes in the separation and orientation of its reflecting surfaces. This stability was essential in the carbon monoxide experiment as significant temperature fluctuations invariably occured during the long accumulation times (usually between 4 and 24 hours) needed to obtain the Brillouin spectra. Since a drift in the plate separation of even one part in 10^6 could seriously reduce resolution, it was essential that thermal expansion effects in the interferometer components be minimal. This condition was achieved in part by having virtually all metal components made from a special iron-nickel alloy (trade name super-Invar)

with a near zero coefficient of linear expansion. As well, the reflecting plates were held in position using a thermally stable mounting system and the material used in the piezoelectric stacks was chosen to have low thermal expansion. Some thermal drift in the interferometer was nevertheless observed, but an electronic stabilization system (see following section) could readily compensate for its effects. Thus no special precautions were taken to regulate the temperature of the Fabry-Perot or its surroundings.

In order to observe the spectrum of the scattered light it was necessary to scan the peak transmission frequency of the Fabry-Perot through a given range. The scanning was done by making small continuous variations in the plate separation with the aid of three piezoelectric stacks arranged in a triangular pattern behind the rear reflector. As a consequence of the condition for constructive interference of light traveling parallel to the axis of a Fabry-Perot,

$$m\lambda \equiv \frac{mc}{\nu} = 2d \qquad 3\text{-}2$$

the frequency, ν, was scanned in inverse proportion to the plate separation, d. The piezoelectric elements were designed to respond linearly to a given bias voltage thus enabling the frequency passed by the interferometer to be accurately correlated with the voltage applied by an external ramp generator. Details of the electronic scanning system will be discussed in the following section. In controlling the plate separation, a common voltage was applied to all three piezoelectric stacks. By applying a separate voltage to each individual element, an arbitrary adjustment could be made to the orientation of the rear Fabry-Perot plate. This capability was useful for electronically controlling the alignment of the reflectors.

proper alignment was a critical factor in maximizing the resolution and the peak transmission obtainable from the interferometer.

Changes in the plate separation and alignment, which were too large to be made with the piezoelectric controls, could be made manually. A triangular arrangement of three very fine adjustment screws enabled the position and orientation of the front plate to be varied over a considerable range. As well, the rear plate assembly could be loosened and allowed to slide lengthwise along its supporting rods thus enabling the plate separation, d, to be set at any value between zero and fifteen centimeters. Setting d at a particular value determined the free spectral range (FSR) of the interferometer. The FSR is defined as the apparent frequency separation between adjacent orders of interference and is given by $\nu'-\nu$ where ν satisfies equation 3-2 for an integer, m, and ν' satisfies the same equation for m+1. Thus:

$$FSR = \frac{c}{2d} \qquad 3\text{-}3$$

All frequency shifts observed in this experiment were measured relative to the free spectral range. Hence an accurate knowledge of the plate separation was required. This was obtained by using a micrometer screw mechanism to move a ball bearing back and forth ten times between the plates. The ball bearing was mounted on a thin rod connected to a piezoelectric transducer driven by a sawtooth waveform. Each time the ball bearing contacted a plate, a clearly observable change occured in an oscilloscope display of the voltage across the transducer. The twenty measurements of plate separation were found to be consistant to within better than 1 part in 1000. Two different free spectral ranges, 11.52 GHz

and 11.10 GHz, were used in the course of this experiment.

The minimum frequency spacing of two spectral lines, which can be resolved by a Fabry-Perot, is directly proportional to the free spectral range of the interferometer (Born and Wolf 1964). The constant of proportionality, (written 1/F), is dependent on several factors, the most significant ones for this experiment being the flatness of the reflectors, the accuracy with which the reflectors were aligned, and the reflection coefficient of the surfaces. The parameter, F, is known as the finesse and is defined to be the ratio of the free spectral range to the half-width of a perfectly monochromatic spectral line when resolved by the Fabry-Perot. Formulas for calculating theoretical finesse are given in Born and Wolf (1964). From these, the contribution due to plate reflectivity was found to be $F_1 = 43$ (reflection coefficient of plates = .93) and the finesse due to imperfections in the plates (rated as being flat to within $\lambda/200$) was estimated at $F_2 = 100$. Assuming the plates were held in perfect parallel alignment, a net finesse of 40 (calculated as in Burleigh "Tech Memo" # FP 140 475) could then be expected. For purposes of comparison with the experimentally observed finesse, this figure had to be multiplied by 1.96 to account for the beam being triple-passed (Sandercock, 1971) through the Fabry-Perot. The resulting theoretical finesse of 78 was somewhat higher than the experimental finesse, about 60, which was usually observed. The difference could most likely be accounted for by imperfect plate alignment, although slight mismatch in the piezoelectric drives and a small amount of electronically induced broadening (see section 3.4) of the peaks may also have been factors. Using the observed value for the finesse, the minimum resolvable frequency separation was calculated

to be of the order of .2 GHz. The closest lines actually resolved in the course of the experiment were separated in frequency by about .3 GHz.

The triple pass option (Burleigh model RC-22) on the RC-10 Fabry-Perot enabled an incident light beam to be sent through the interferometer three times before emerging. This had the effect of improving the ability of the Fabry-Perot to simultaneously display two spectral lines differing greatly in intensity. Since complete destructive interference never occurs in a Fabry-Perot (for the same reasons that the finesse is finite), some fraction of the light incident at a given frequency, is transmitted regardless of the plate separation. The ratio of the maximum transmitted intensity to the minimum transmitted intensity is known as the contrast, C, and is a function of the finesse (Sandercock, 1971). For single pass operation, the contrast of the Fabry-Perot used in this experiment was calculated to be about 650. Thus a peak of height, h, would unavoidably be accompanied by a "background" of height h/650. The spectral lines corresponding to Brillouin scattering from transverse elastic waves in carbon monoxide were frequently observed to have less than 1/1000 the intensity of the unshifted line at the laser frequency (Rayleigh line). Thus, in many cases, single pass operation of the Fabry-Perot would not have enabled these lines to be detected.

Triple passing light through a Fabry-Perot caused the resultant transmission coefficient (ratio of transmitted intensity to intensity incident on the interferometer) to be raised to the third power (analogous to passing light through three consecutive optical filters). This result does not depend on whether constructive or destructive interference occurs. Hence, both the maximum and minimum transmission coefficients are cubed and

therefore the contrast is cubed. Thus using the triple pass option on the RC-10 yielded a theoretical contrast of better than 10^8. This high contrast could not be observed in practice due to a variety of factors, unrelated to the interferometer, which tended to build up the background. Nevertheless, Brillouin peaks with intensities only 10^{-4} that of the Rayleigh line were clearly observable with the aid of the triple pass system.

Since the alignment of the Fabry-Perot had a critical effect on its performance, especially in the case of the multipass system, considerable care was taken in aligning the instrument at the beginning of the experiment. In the first stage of the alignment procedure, the Fabry-Perot (set for single pass operation) was positioned so that its reflecting surfaces were approximately perpendicular to the optic axis defined by the He-Ne laser beam. This condition was indicated when the beam was reflected back on itself by the rear Fabry-Perot plate. The plates were then made roughly parallel by using adjustment screws to vary the orientation of the front plate until only a single beam (combining all multiple reflections) emerged from the interferometer. More precise alignment was achieved by replacing the He-Ne beam with a point source of light (provided by focusing the argon laser beam on a white card) and then adjusting the front plate to yield a pattern of circular fringes. A repeating ramp voltage (scanning at about 1 FSR per second) was subsequently applied to the piezoelectric drives on the rear plate and a lens was inserted in front of the interferometer to collimate the incident light. Reasonably good alignment was indicated if the light transmitted by the interferometer formed a single flashing spot.

After reducing the source brightness by placing filters in the

argon laser beam, the transmitted light could be monitored using the photomultiplier detection system. The peaks displayed on the CRT of the DAS unit, while initially quite broad, could readily be narrowed (to indicate a finesse of 20 or 30) by using the adjustment screws controling the front plate. The card used to scatter the laser beam was then removed and the lens in front of the interferometer was repositioned so as to focus on the cell. The laser beam was directed through the cell but was aimed so that it struck the quartz wall thus providing sufficiently intense scattering to form clearly observable peaks on each scan across the DAS display. The single pass finesse was then maximized, first by using the adjustment screws and then by making fine adjustments to the bias voltage on the piezoelectroc elements controling the orientation of the rear plate. Once a finesse of between 30 and 40 was observed, the interferometer was switched over to triple pass operation.

It was essential to have very precise alignment of the interferometer plates before attempting to use the triple pass option. This resulted from the fact that, in making three passes through the interferometer, light traveled along paths displaced laterally from one another by several millimeters. Hence, a misalignment of the plates caused differing values of the apparent plate separation, d (as in equation 3-2), for each pass, with the result that no frequency, ν, satisfied the condition for constructive interference on all three passes. Thus, when even slightly misaligned, the triple pass system would not transmit any light. A similar effect could have resulted if the three light paths were not highly parallel. However, this possibility was eliminated in the design

of the triple pass system, by using corner cube retroreflectors to make the two necessary reversals in the beam direction. Corner cubes consist of three mutually perpendicular (to within a few seconds of arc) mirrors, intersecting to form a corner. It can be shown geometrically that a ray of light, reflected once from each internal surface of a corner cube, will undergo a translation and a precise reversal in direction, regardless of the angle of incidence. Alignment of the two corner cubes was therefore not critical, and they could be satisfactorily held in loose plastic mounts, one of which was rotatable to allow easy conversion from single pass to triple pass operation.

Since the transmitted intensity was such a strong function of alignment, it was relatively simple to use the piezoelectric adjustments to optimize the transmission (and simultaneously the finesse) of the triple pass system. Appropriate adjustments, however, depended on at least some transmitted light being observed, thus necessitating the preliminary single pass alignment. Once good triple pass finesse (about 60) was obtained, the automatic stabilization feature of the DAS unit was used to maintain the finesse while a Brillouin spectrum of CO was recorded.

The complete Fabry-Perot alignment procedure, beginning with the use of the He-Ne laser beam, had to be carried out just once, at the start of the experiment. However, the part of the procedure involving only the piezoelectric controls, and beginning with the scattering of the argon laser beam from the cell wall, was performed routinely. This was made necessary because of thermal drift in the Fabry-Perot, which, if uncompensated could substantially reduce or eliminate triple pass transmission in less than half an hour. Thus, partial realignment was necessary each

time the Fabry-Perot was used following its being disconnected from the stabilization system for any appreciable length of time.

The light transmitted by the interferometer was directed by way of a lens (focal length = 100 cm) and a pinhole to a photomultiplier tube. The pinhole was placed at the focus of the lens to insure that all light reaching the photomultiplier was traveling very nearly parallel to the optic axis. Light deviating from the axis traveled a slightly lengthened path between the interferometer plates and hence satisfied the condition for constructive interference at a smaller plate separation than that required for light traveling parallel to the axis. This effect could have resulted in a decrease in finesse. The diameter of the pinhole (1.0 mm) was therefore chosen to eliminate any angular deviation sufficient to cause a noticable reduction in finesse, while still allowing a reasonably large fraction of the incident light to be tramsmitted. The lens was held in place using an x-y mount which enabled fine adjustments to be made in the position of the beam leaving the interferometer. The photomultiplier (Electro-optical Div. ITT, model ITT FW 130) featured high sensitivity and a low dark count (~1 per second) when cooled thermoelectrically. It thus provided an accurate means of monitoring the very low light intensities encountered in the experiment. The output of the photomultiplier was connected, by way of an amplifier - discriminator, to the DAS unit. The light detection system and the interferometer were housed together beneath a large opaque enclosure (made from styrofoam, painted black and covered with black cloth) to minimize possible effects from extraneous light.

3.4 DAS System and the Recording of the Brillouin Spectrum of β-CO

The data aquisition and stabilization system, DAS-1, is an electronic system designed by Burleigh Instruments Inc. expressly for use with a piezoelectrically scanned Fabry-Perot interferometer. The unit performs three primary functions. It generates a ramp voltage which scans the interferometer plate separation through a given range. It employs a multichannel analyzer to accumulate digital data on the light intensity transmitted by the interferometer. It then uses this data in making automatic adjustments which maintain proper average separation and alignment of the Fabry-Perot plates. In addition, the DAS incorporates a number of special features, enabling it to be adapted to a wide variety of experimental circumstances. The DAS features pertinent to obtaining the Brillouin spectrum of CO are illustrated in the following block diagram (figure 5).

The DAS system stored experimental data (photon counts vs. frequency passed by the Fabry-Perot) using a multichannel analyzer (MCA) having 1024 channels, each able to accomodate up to $2^{24} - 1 = 16777215$ counts. The ramp waveform generated by the DAS was used simultaneously in scanning the separation of the Fabry-Perot plates and in sweeping the channel address scaler (electronic pointer designating the channel in which counts will accumulate) through the 1024 channels. By making the plate separation a linear function of the ramp voltage, a given channel was made to correspond to a particular plate separation and hence a particular frequency passed by the Fabry-Perot. The linear relation between frequency and channel number was independent of the ramp waveform.

Burleigh Instruments Inc. DAS-1

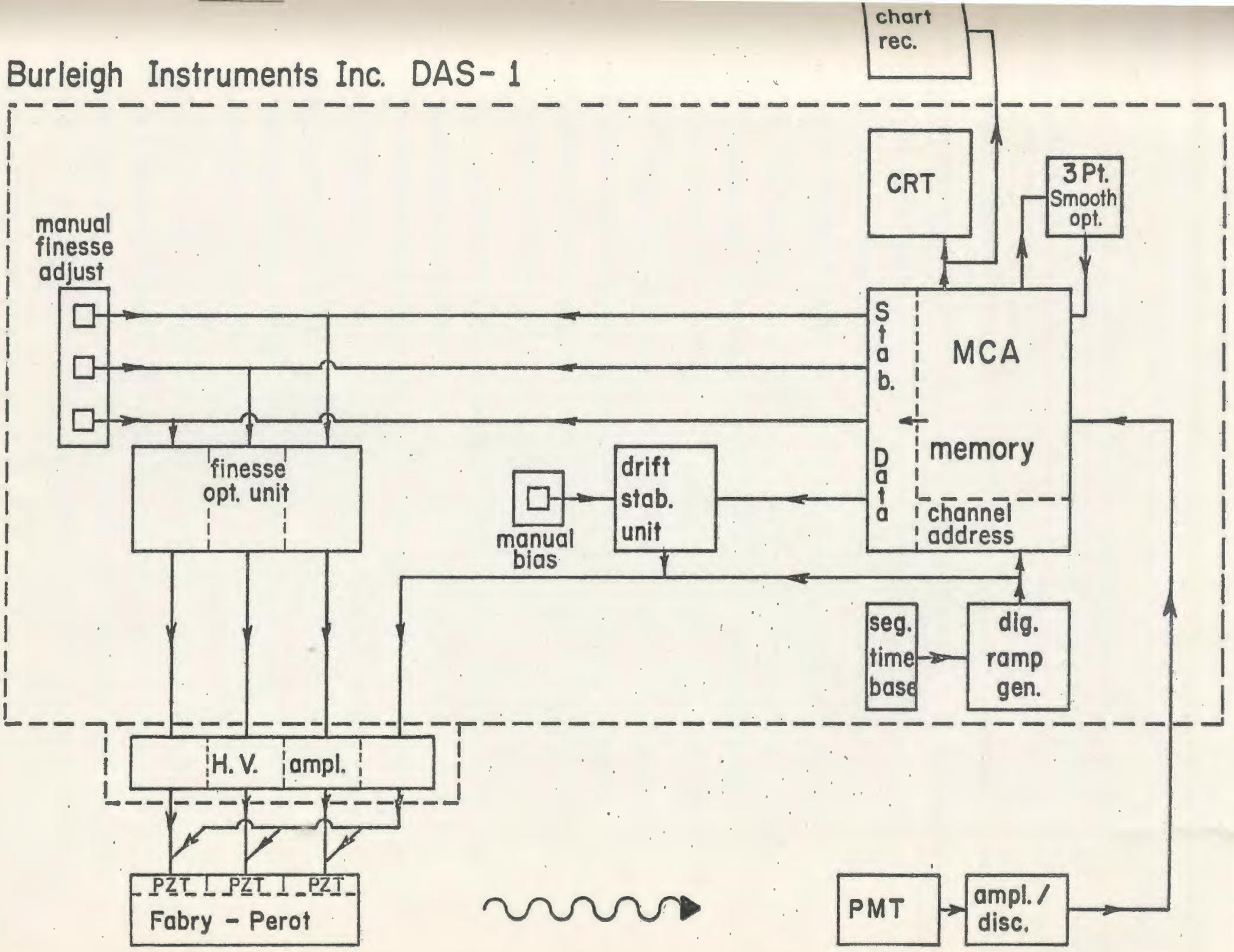

The ramp waveform did, however, determine the amount of time spent by the system in accumulating data at a given plate separation. In the ordinary mode of operation, equal time was spent on each channel. This was accomplished by increasing the ramp voltage in a series of discrete steps, each having equal magnitude and duration. The ramp waveform (referred to as a digital ramp) thus resembled a staircase, the steps of which simultaneously advanced the Fabry-Perot plate separation by a fixed amount and advanced the channel address scaler by one channel. The duration of the steps corresponded to the time spent per channel or "dwell time" and could be adjusted by increments of .01 ms from .01 ms to 99.99 ms. After the channel address scaler reached channel 1024, count accumulation in the MCA was prevented while the address scaler counted back down to the first channel at a rate of .01 ms/channel. Then, following a delay of 2 ms, to allow the piezoelectric elements and Fabry-Perot plates to settle down, a new sweep was begun.

An optional feature, known as the segmented time base, enabled the dwell time for each channel in an arbitrarily chosen group, to be increased by a factor between 1 and 99. The system could thus be made to spend the majority of its time accumulating data in one or more frequency intervals representing particularly interesting regions of the spectrum. An example provides the best means of illustrating the usefulness of this feature. Figure 7 shows a Brillouin spectrum of CO where the segmented time base was used to increase the dwell time for channels 510 to 528 and 561 to 620, by a factor of 50. Channels 510 - 528 were included in the slowly scanned region in order to facilitate stabilization (to be discussed shortly). The effect of the increased dwell time on the channels, 561 - 620,

was to make the two very low intensity lines appearing in that interval (formed by scattering from transverse elastic waves) clearly visible after a total spectrum accumulation time of 21.7 hours. Of this time, 12.7 hours (59%) were spent accumulating counts in the interval containing the lines, 4.6 hours (21%) were spent on the stabilization interval, 4.1 hours (19%) were spent on the remainder of the spectrum and the rest of the time, .3 hours (1%) was spent on the flyback portion of the ramp. To achieve the same signal to noise ratio in the transverse lines without the use of the segmented time base, would have required a total accumulation time of 220 hours (9.2 days). For a variety of reasons, it would have been very difficult, if not impossible to keep the experiment running continuously for this length of time.

The DAS provided two independent modes of stabilization of the Fabry-Perot cavity. The drift stabilization module controlled the mean plate separation by applying a common bias to all three piezoelectric elements in the Fabry-Perot, while the finesse optimization module applied individual biases to make appropriate adjustments in the plate orientation. The drift stabilizer worked by locking a relatively narrow and intense spectral line to a given position in the MCA memory. This position was designated by setting an electronic flag in each of three MCA channels. The first flag could be set in any channel (except those lying close to 1 or 1024) and was used to specify the location of the centre of the stabilized line. The next two flags were set as a pair, symmetrically located about the centre, and were used to mark off an interval of channels which formed the drift stabilization window. This window was generally chosen to have a width about equal to the half-width of the line used for

stabilization. Drift of the stabilization line was detected by monitoring the relative rates of count accumulation in the two halves of the stabilization window. After each cycle of the ramp waveform, the difference in the number of counts added to the upper and lower halves was automatically calculated. The sign of this difference indicated the direction of drift of the line (due either to drift in the source frequency or thermal drift in the Fabry-Perot) and hence directed the DAS in making an appropriate bias correction step. The magnitude of a correction step was specified at the beginning of an experiment and could be chosen from the values 1, ½ ... ... 1/16 (in arbitrary units). In picking the value, a compromise was made between the possibility of broadening the lines by having the correction steps too large and the possibility of having the steps too small to keep up with the maximum likely rate of drift.

The DAS optimized the Fabry-Perot finesse by using a routine similar to that used for drift stabilization, although slightly more complicated. A single window, centred on the channel at the centre of the drift stabilization window, was established by setting another pair of electronic flags. The lower channel in which a flag was set formed the lower boundary of the optimization window. This channel could be selected from any of the channels in the lower half of the stabilization window, but was usually chosen so as to make the optimization window quite narrow. The finesse was monitored by using the combined count per ramp cycle in the channels comprising the optimization window as a criterion. Assuming constant source intensity, this count provided a good measure of both the height of the peak and the degree to which counts were concentrated in the centre. Drift in the plate alignment would cause a decrease in the

count rate in the optimization window but would not provide an indication as to the nature of an appropriate correction step. The DAS thus employed test steps in which the biases on the piezoelectric elements were systematically altered so as to change the alignment of the Fabry-Perot plates in a known manner. The effect of the test step on the finesse indicated the direction of an appropriate correction step.

Four ramp cycles (labeled sweep 1 .... sweep 4 in the following discussion) were required to complete one full cycle of the finesse optimization routine. The routine began with a test step, made at the end of sweep 1 which tilted the reflectors about a vertical axis. At the end of sweep 2, a comparison was made between the number of counts accumulated in the optimization window during sweep 1 and the number accumulated during sweep 2. The test step was then nullified and a correction (of smaller magnitude then the test step) was applied in the same direction as the test if the comparison indicated an increase in finesse, and in the opposite direction otherwise. The second half of the routine, consisting of test and correction steps made at the end of sweeps 3 and 4 respectively, differed from the first half only in that the reflectors were tilted about a horizontal axis. Test and correction step magnitudes were selected at the beginning of an experiment using a similar criterion to that used in choosing the drift stabilization correction. Possibilities for the test step were 1, ½ .....1/16 (in arbitrary units) while the correction step could be set at a fraction, 1/4, 1/8 or 1/16, of the test step.

During an experiment the data accumulated in the MCA memory was displayed continuously on the DAS cathode ray tube (CRT). The display showed a spectrum consisting of counts (proportional to intensity) on the

y axis versus channel number (proportional to frequency) on the x axis. The display also provided alpha-numeric readout of the exact count in a given channel. This was obtained by positioning the "bug" (luminous dot having a brightness greater than the dots forming the spectrum) in a desired channel and then reading both the channel number and the exact count in that channel from a digital display at the top of the CRT screen. Positioning the bug in channel zero provided a digital readout of the number of sweeps made by the DAS. The drift stabilization window and finesse optimization window were indicated in the display by vertical bars and intensified spots respectively. Intensified spots also marked any slowly scanned intervals of channels formed by application of the segmented time base feature. At the conclusion of an experiment, the spectrum displayed on the CRT could be recorded in graphical form on a Hewlett-Packard model 7133 A chart recorder.

The experimental procedure used in obtaining Brillouin spectra of CO consisted primarily of the optical alignment described in the previous section, followed by appropriate programming (setting windows, correction steps etc.) of the DAS unit. The DAS was then able to accumulate data automatically for several hours with little or no adjustment. An important consideration at the beginning of an experiment was the laser beam intensity incident on the crystal. This could be varied from about ten milliwatts up to almost one watt by either controlling the current supplied to the plasma tube in the laser, or by attenuating the laser beam with filters. High intensity allowed reduced accumulation times for the Brillouin spectra, but caused a large increase in the probability of having absorbed light destroy the CO crystal (see discussion

in previous section). It was thus found advantageous to work quite near the low end of the laser power range. A visual inspection of the intensity of light scattered from the cell was the most useful method of initially determining whether or not a "safe" amount of light was being passed through the crystal. The scattered intensity was a function of both the incident intensity and the optical quality of the crystal, the latter factor being of major importance in initially estimating the risk of damage. Degrading of the optical quality during an experiment was indicated if a routine check of the DAS display revealed large increases in the rate of count accumulation in the channels corresponding to the laser frequency. In many cases this necessitated terminating the accumulation of data for a given spectrum.

Standard stabilization and optimization windows were used in obtaining most of the Brillouin spectra of CO. These windows centred the peak of a given order of the Rayleigh line on a channel (number 519) chosen near the midpoint of the set of 1024 channels. The width of the drift stabilization window was fifteen channels (about the half width of the Rayleigh line) while the finesse optimization window was 5 channels wide. The finesse correction and test steps and the drift correction step were set at their minimum values in most cases. This necessitated a fairly small period for the ramp cycle so that corrections (occuring at the ends of the sweeps) would be made frequently enough to keep up with any drift which might occur. Simultaneously, however, a sufficiently long dwell time had to be allowed to enable a statistically useful number of counts (at least ten in the centre channel) to accumulate in the stabili-

stabilization channels on each sweep. The compromise usually involved a dwell time of between .5 ms and 5 ms (depending on the intensity of the Rayleigh line) for the channels used in stabilization. Whenever the segmented time base was employed, the stabilization windows were included in the region of extended dwell time to ensure that the conditions necessitating the above compromise were satisfied.

The various spectra obtained in the experiment could be divided into two categories depending on whether the main objective was to pinpoint the longitudinal or the transverse components of the Brillouin spectrum of CO. The spectra intended primarily for determining longitudinal shifts were accumulated in between one and five hours and had of the order of a few hundred thousand counts per channel at the peak of the Rayleigh line. The longitudinal lines were clearly visible with a few thousand counts in their centre channels; in several cases one of the transverse lines a few hundred counts high was also visible above the background. The background count was typically of the order of 40 counts/second on several spectra made when admitting light of all frequencies to the optical detection system. In spectra recorded in the latter stages of the experiment, the background was reduced to about 6 counts/second by using an interference filter to limit the frequency of the detected light to a value near the laser frequency. The interference filter had a bandpass of 2300 GHz, centred at the laser frequency, and was located on the optic axis between the cell and the front pinhole. Primary contributions to the background included the photomultiplier dark count, extraneous light in the room and scattered laser light, shifted in frequency by Raman scattering in CO.

The intensity of scattering in the longitudinal Brillouin components was strongly dependent on the polarization of the incident laser light. Thus, to facilitate observation of the longitudinal lines, a half wave plate was positioned in front of the laser. This rotated the plane polarized laser output to yield polarization of the beam through the crystal in the x-z plane (coordinates as in figure 2). This polarization was the most favourable for observing scattering from longitudinal elastic waves but appeared to be a significant disadvantage when attempting to observe the transverse components. The rotator was therefore used only when recording spectra intended mainly for locating the longitudinal lines. In the absence of the rotator the beam through the crystal was polarized in the y-z plane.

The spectra used primarily for locating transverse components required long accumulation times due to the low intensity of the transverse lines relative to the background. It was generally found necessary to use the segmented time base feature (discussed previously), combined with total data accumulation times ranging between 15 and 25 hours, before the transverse components could be accurately pinpointed. Typically, spectra recorded in these time intervals had between 1 and 5 million counts at the peak of the Rayleigh line and showed transverse peaks a few hundred counts above a background of a few thousand counts. In only a few cases were both transverse components (T1 and T2) resolvable simultaneously on a single spectrum. In several instances it would have been desirable to collect data for periods exceeding 25 hours. However, this time appeared to represent a practical limit on the ability of a CO crystal in this experiment to survive the effects of the laser beam without being seriously

damaged.

Each of the carbon monoxide crystals grown in this experiment yielded several spectra, recorded at differing angles of rotation of the cell about the z axis (axis of the rotation mechanism in the cryostat). In the earlier stages of the experiment, the cell rotation angles were chosen arbitrarily. First a spectrum was recorded at some particular angle setting on the indicator at the top of the cryostat, and then subsequent spectra were recorded at angle settings differing from the initial setting by 10 or 20 degree intervals. Later in the experiment, the cell rotation angle was set specifically to yield desired values of the angle γ (see section 3, chapter 1). This procedure proved much more useful in obtaining the values of γ needed to pin down the frequency shift vs. γ curves (see figure 8) and hence the elastic constants. γ was given in terms of the Euler angles of the crystal by the expression:

$$\cos\gamma = \frac{1}{\sqrt{2}} \left(\sin\theta \cos\phi + \cos\theta\right) \qquad 3\text{-}4$$

In general, the values of γ obtainable from a given crystal by rotating it about the laboratory frame z axis were restricted to a limited range which did not include all angles between 0^{o} and 90^{o}. The combination of all crystals used in the experiment, yielded γ values ranging from 9^{o} to 85^{o}.

After concluding data accumulation at a given crystal orientation, the resulting Brillouin spectrum was output on the chart recorder connected to the DAS. The relevant digital data was then obtained from the CRT display and was recorded on the spectrum produced by the chart recorder. Depending on whether or not the crystal was still of satisfactory optical quality, it was either melted or else was rotated to a new orientation

before beginning another spectrum. A total of 35 Brillouin spectra yielding 60 data points (frequency shifts of L, T1 or T2 components) were recorded using 7 crystals grown in the course of this experiment.

CHAPTER 4

RESULTS

4.1 The Brillouin Spectrum of β-CO

Several common features were shared by the various Brillouin spectra of β-carbon monoxide. In all cases, the Fabry-Perot interferometer was scanned through approximately 3.5 free spectral ranges, thus making the Rayleigh line visible in three orders. The Rayleigh line was invariably the most intense spectral feature and was presumed to be primarily a consequence of scattering from various surfaces (dust particles, flaws in the crystal, liquid - solid interface, etc.) in the sample cell. Three Brillouin components were observed in the spectra. These resulted from scattering by the longitudinal and the two transverse modes of elastic waves propagating in a crystal of CO. The Brillouin lines appeared in pairs, symmetrically located about the Rayleigh line, corresponding to the positive and negative values of Ω referred to in section 3, chapter 1. Both the upshifted and downshifted longitudinal lines were visible in two orders while the transverse lines, when visible, appeared in three orders. Representative Brillouin spectra, showing the various components, appear in figures 6 and 7.

Although the spacing between the adjacent orders of the Rayleigh line should supposedly have been equal, a discrepancy of one or two channels was sometimes noticed. This probably implied a small degree of non-linearity in either the DAS high voltage amplifier or in the response of the piezoelectric stacks. To minimize possible errors, the frequency shift of

Figure 6 - Representative Brillouin spectrum of β-carbon monoxide

R - Rayleigh line
L - Longitudinal Brillouin line
T_2 - Second transverse Brillouin line

The labeled Brillouin lines are the upshifted and downshifted components associated with the labeled Rayleigh line.

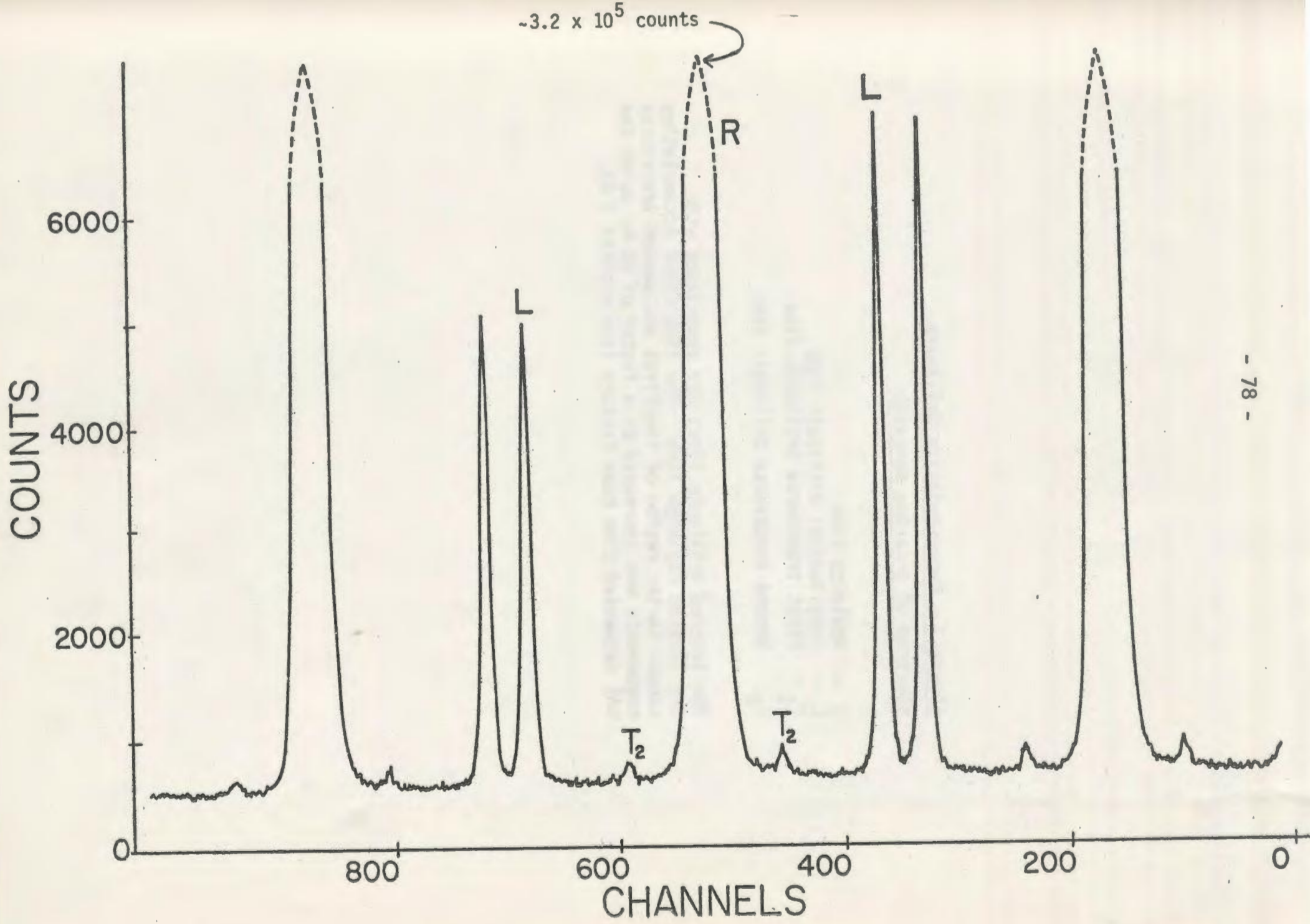
~3.2 x 10^5 counts
R
L
L
L
T2
T2
6000
4000
2000
0
COUNTS
800
600
400
200
0
CHANNELS

Figure 6

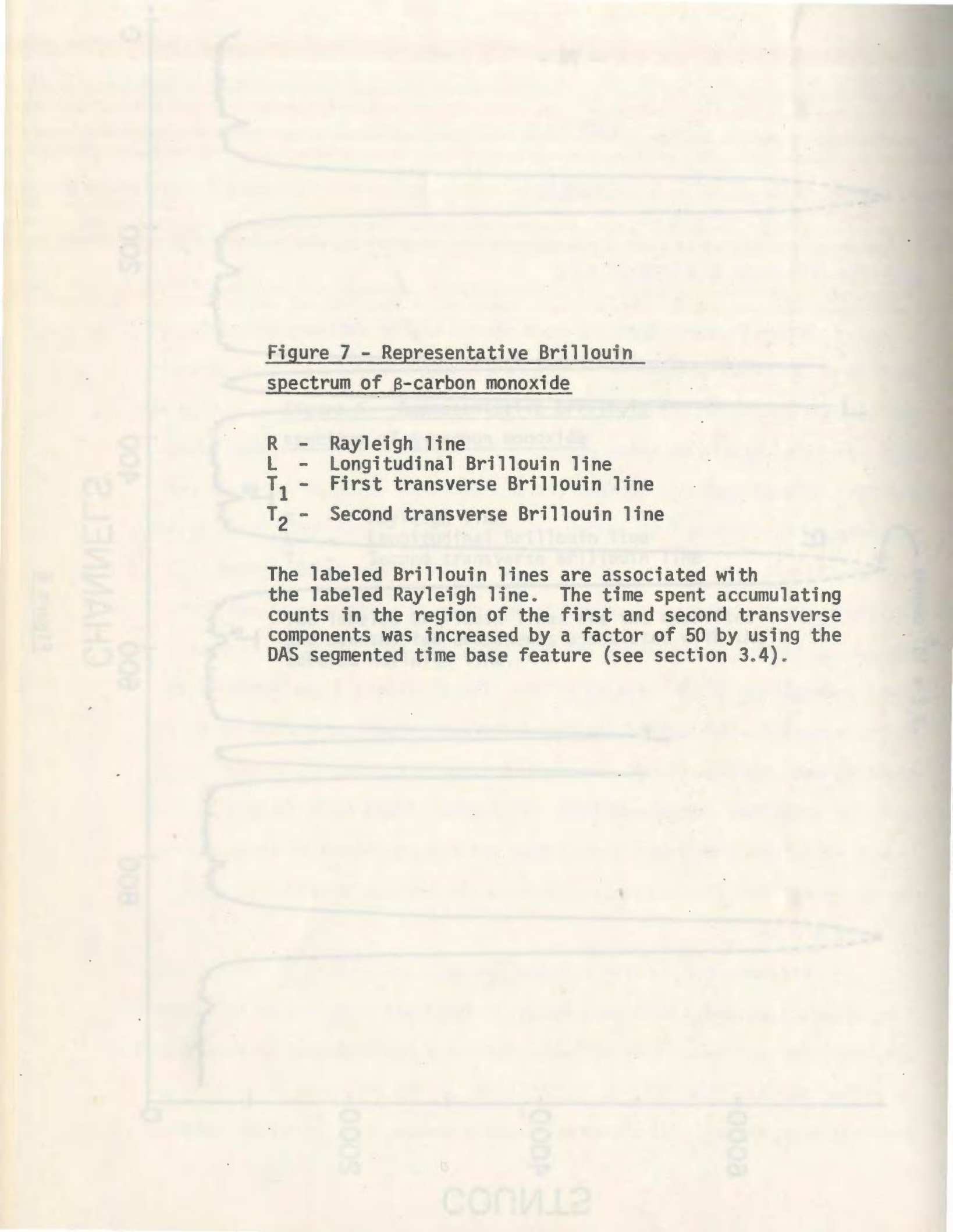

Figure 7 - Representative Brillouin spectrum of β-carbon monoxide

R - Rayleigh line
L - Longitudinal Brillouin line
T_1 - First transverse Brillouin line
T_2 - Second transverse Brillouin line

The labeled Brillouin lines are associated with the labeled Rayleigh line. The time spent accumulating counts in the region of the first and second transverse components was increased by a factor of 50 by using the DAS segmented time base feature (see section 3.4).

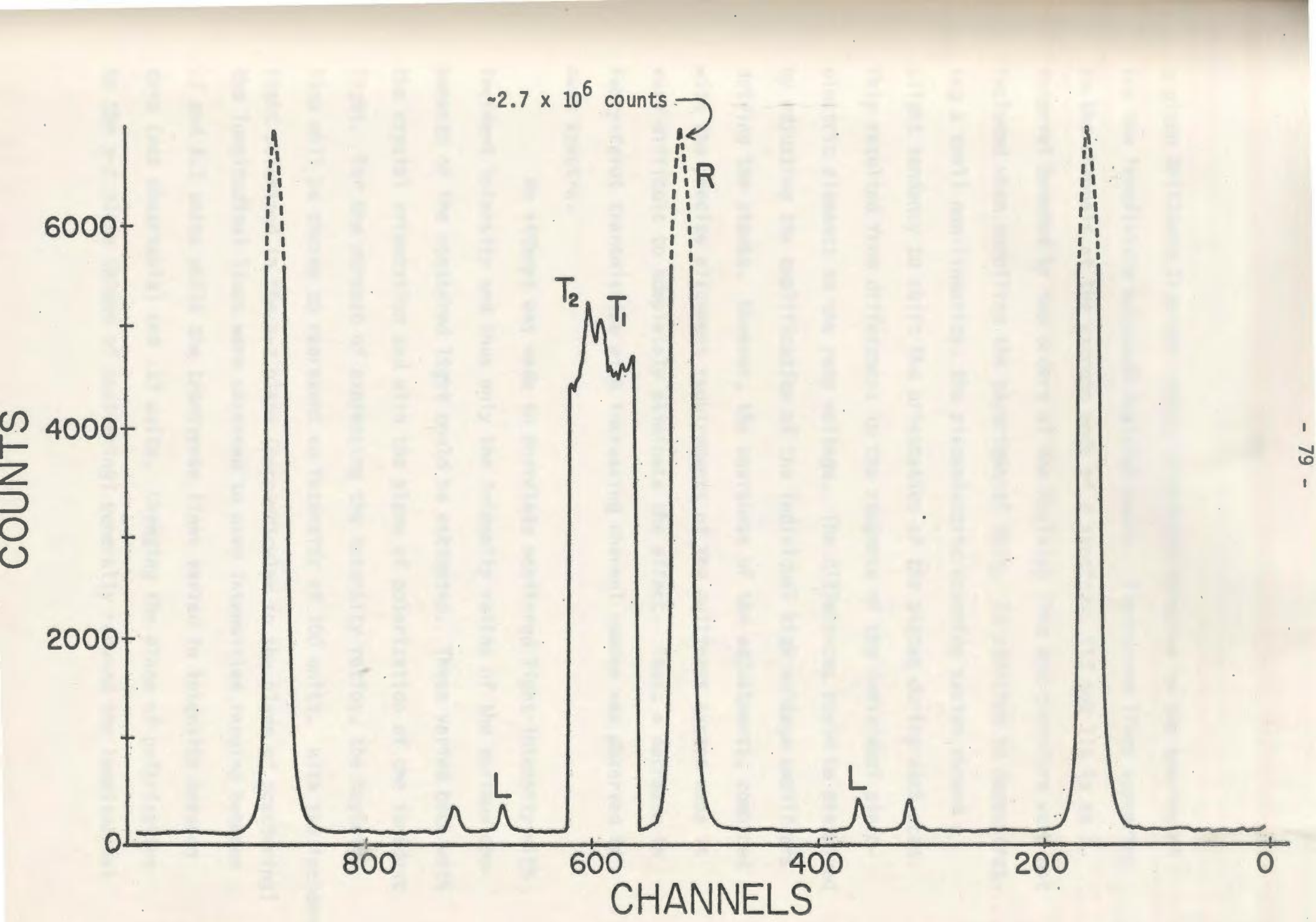
~2.7 x 10^6 counts
R
T2
T1
L
L
6000
4000
2000
0
COUNTS
800
600
400
200
0
CHANNELS

Figure 7

a given Brillouin line was always calculated relative to the spacing of the two immediately adjacent Rayleigh peaks. Transverse lines appearing in the channels at the extreme ends of a spectrum, did not lie in an interval bounded by two orders of the Rayleigh line and therefore were not included when compiling the experimental data. In addition to demonstrating a small non-linearity, the piezoelectric scanning system showed a slight tendency to shift the orientation of the plates during each scan. This resulted from differences in the response of the individual piezoelectric elements to the ramp voltage. The differences could be minimized by adjusting the amplification of the individual high voltage amplifiers driving the stacks. However, the coarsness of the adjustments, combined with the precise alignment requirements of the multipass system made it very difficult to completely eliminate the effect. Thus, a decrease in Fabry-Perot transmission with increasing channel number was observed in most spectra.

No attempt was made to correlate scattered light intensity with incident intensity and thus only the intensity ratios of the various components of the scattered light could be estimated. These varied both with the crystal orientation and with the plane of polarization of the incident light. For the purpose of expressing the intensity ratios, the Rayleigh line will be chosen to represent an intensity of 100 units. With the incident light polarized in the x-z plane (perpendicular to the plane of scattering) the longitudinal lines were observed to have intensities ranging between .7 and 4.3 units while the transverse lines varied in intensity between zero (not observable) and .17 units. Changing the plane of polarization to the y-z plane (plane of scattering) generally reduced the longitudinal

intensities by a factor of about 4 yielding a range of values lying between .10 and 1.22. The effect of the polarization on the transverse line intensities was not well determined in this experiment. It was noted, however, that simultaneous appearance of both transverse components was observed only when the incident light was polarized in the plane of scattering. With this polarization, the maximum observed intensity of a transverse line was .06 units. The ratio of the intensities of the two transverse lines was highly variable but usually was such that only one of the lines was clearly visible on a particular spectrum. In the few cases where the transverse components had nearly equal strength, the intensity of both the lines was observed to be substantially reduced.

It is interesting, at this point, to briefly compare the intensity of the β-CO Brillouin spectrum with the Brillouin spectrum observed for β-N_2 (see Kiefte and Clouter, 1975). Although many properties of the two substances are found to be remarkably similar (see for example, section 4, chapter 4), this similarity vanishes when considering the Brillouin scattering intensities. Expressed on a scale analogous to that used above, the intensities of the β-N_2 Brillouin components are observed to be of the order of 30 units for the longitudinal peaks and 5 units for the transverse peaks. These ratios are, on average, around 10 to 100 times greater than those for β-CO. The contrast in the actual intensities of the Brillouin components was likely an order of magnitude greater than this due to β-N_2 having a much stronger Rayleigh component (estimated visually) than β-CO. No further discussion of this observation will be included here since the factors governing the scattering intensities lie outside the realm of the present investigation. However, it can be noted that the intensity

of the β-N_2 Brillouin spectrum is quite typical of that of a variety of molecular crystals and consequently, the very low intensities observed in the β-CO spectra represent a distinct anomaly.

Before the frequency shift data from the various Brillouin spectra could be tabulated, it was necessary to classify the Brillouin components as either L, T1 or T2, and to determine with which order of the Rayleigh line, the components were associated. Comparison of the β-CO Brillouin spectrum with the fully analyzed Brillouin spectrum of β-N_2 (Kiefte and Clouter, 1975) provided a rough indication of what the expected frequency shifts might be. This substantially reduced ambiguity in analyzing the spectra as it allowed initial choice of a free spectral range which virtually eliminated the possibility of overlapping of orders. It was thus necessary only to determine if a given longitudinal line belonged to the nearest or second nearest adjacent Rayleigh line. By slightly decreasing the free spectral range during the course of the experiment, and observing that the longitudinal components moved closer together, it was established that each longitudinal component was associated with the order of the Rayleigh line lying nearest to it.

Although a longitudinal line was easily recognizable by its relatively high intensity and large shift, there was no simple way to determine whether a transverse component was T1 or T2. This ambiguity presented a significant obstacle to analyzing the data and was found to persist even after a fairly large volume of data had been accumulated. Trial and error was used to classify the transverse lines, with the proper classification being indicated by a good fit between the experimental data and theoretical curves of the form specified by equations 1-39. The theoretical curves were

fit to the data using a least squares procedure (see following section). The minimum value obtained for the total squared error indicated the goodness of the fit and thereby the validity of the transverse line assignments. At the intended conclusion of the experiment, it was noted that the majority of the transverse lines fell distinctly into one or the other of two sets. Fits of nearly equal quality were obtained if either all lines in one set were labeled T1 and the others labeled T2, or if this labeling was reversed. Resolution of the ambiguity required knowledge of the longitudinal frequency shifts at low values of the angle γ. Thus, a final crystal was grown, and with some very good luck (the crystal happened to grow at a highly favourable orientation) the necessary data (longitudinal shifts for γ as low as 9^0) were obtained. Table 1 shows the entire set of frequency shift data obtained from all of the Brillouin spectra.

4.2 Determination of the Elastic Constants

A combination of the wave velocity equations (equations 1-39) and the Brillouin equation (equation 1-41) provided the relations used in determining the elastic constants of β-CO from Brillouin scattering data. The initial analysis of the experimental data was performed without knowledge of some of the multiplicative parameters (in particular, the refractive index, n, and the density, ρ) appearing in equations 1-39 and 1-41. For this reason, and to facilitate the error analysis, the following discussion will treat the question of fitting curves to the experimental data separately from the question of explicitly evaluating the elastic constants.

Curves of the form 1-39 were fit to the experimental data according

Table 1

Ω vs. γ for β-CO

Euler Angles			γ	Observed shifts (GHz)			Calculated shifts (GHz)		
φ	θ	ψ		L	T1	T2	L	T1	T2
179.3	126.0	196.5	9.0	5.205	—	—	5.198	2.149	2.188
193.1	126.0	196.3	13.4	5.185	—	—	5.171	2.151	2.235
203.7	126.0	196.6	20.0	5.115	—	—	5.115	2.155	2.326
212.6	126.3	196.2	26.0	5.054	—	2.462	5.053	2.161	2.419
221.4	125.9	196.8	32.4	4.988	—	2.480	4.984	2.167	2.511
354.6	86.2	191.4	41.5	4.858	2.159	2.559	4.902	2.178	2.595
239.4	126.2	197.1	44.9	4.889	—	—	4.881	2.182	2.605
335.9	86.5	191.6	46.6	4.877	2.189	2.621	4.873	2.184	2.606
188.4	269.0	254.1	46.6	4.858	2.190	—	4.873	2.184	2.606
169.3	268.4	253.5	47.6	4.854	2.186	—	4.869	2.186	2.604
198.5	269.2	254.1	48.7	4.874	—	—	4.866	2.187	2.602
151.2	92.1	69.6	49.8	4.874	2.214	2.598	4.863	2.188	2.597
208.6	269.4	254.1	52.2	4.854	—	—	4.860	2.191	2.584
216.0	269.6	253.9	55.5	4.867	—	—	4.861	2.195	2.555
140.0	13.2	65.9	55.6	4.860	—	—	4.861	2.195	2.554
251.4	23.7	345.3	56.2	4.865	2.208	2.545	4.862	2.196	2.548
137.9	92.3	70.2	56.5	4.881	2.208	2.561	4.862	2.196	2.544
225.5	15.5	65.9	56.7	4.867	—	—	4.862	2.196	2.542
315.4	86.8	191.7	57.2	4.846	2.189	2.498	4.863	2.197	2.536
215.5	15.2	65.5	57.9	4.875	2.185	—	4.865	2.198	2.528
159.6	13.7	66.0	58.0	4.838	—	—	4.865	2.198	2.527
154.9	81.3	93.9	58.3	4.861	2.189	—	4.866	2.198	2.523
205.4	14.9	66.1	58.7	4.867	—	—	4.867	2.199	2.518
178.0	14.1	65.5	59.1	4.862	2.189	—	4.868	2.199	2.513
195.2	14.6	66.6	59.2	4.873	2.208	—	4.868	2.199	2.511
223.3	269.7	253.6	59.3	4.884	—	—	4.869	2.199	2.510
186.6	14.4	66.1	59.3	4.867	—	—	4.869	2.199	2.510
139.7	81.5	94.2	64.6	4.872	—	2.470	4.888	2.205	2.432
181.2	23.1	345.1	68.1	4.918	2.214	—	4.905	2.208	2.375
243.4	270.4	255.0	71.2	4.909	—	2.296	4.919	2.210	2.325
120.9	81.7	94.7	75.1	4.936	—	—	4.937	2.213	2.265
295.7	128.1	196.7	78.8	4.962	—	—	4.952	2.215	2.217
85.1	82.8	94.9	81.5	4.949	—	—	4.961	2.216	2.188
77.6	92.8	71.0	83.3	4.982	2.199	—	4.966	2.217	2.173
105.5	81.5	94.7	85.3	4.970	—	2.167	4.969	2.217	2.160

to a "least squares" criterion. The squared error term, χ^2, which was minimized to yield the least squares fit, was given by:

$$\chi^2 = \frac{1}{D} \sum_i \frac{(\nu_i^{predicted} - \nu_i^{observed})^2}{\sigma_i^2} \qquad 4\text{-}1$$

In the above expression, $\nu_i^{observed}$ denotes a frequency shift measured from a Brillouin spectrum and $\nu_i^{predicted}$ denotes a calculated frequency shift corresponding to the appropriate crystal orientation and to the appropriate type of Brillouin component (i.e. L, T1 or T2). σ_i is the estimated standard deviation of the i'th experimental measurement while the index, i, runs from 1 to 60 corresponding to the 60 data points obtained in the experiment. D is the number of degrees of freedom, this being 56 in the present case. The quantity, $\nu_i^{predicted}$ was calculated directly from the equations 1-39 except that the factor $\rho^{-\frac{1}{2}}$ was omitted. Thus, the expression for $\nu_i^{predicted}$ differed from the "correct" expression for a frequency shift by a multiplicative factor,

$$M \equiv \frac{2n \sin(\alpha/2)}{\lambda\sqrt{\rho}} \qquad 4\text{-}2$$

where α was the scattering angle and λ was the laser wavelength. The parameters which were varied in the course of minimizing χ^2, were analogous to the five elastic constants c_{mn} (mn ≡ 11, 12, 13, 33 or 44) appearing in the velocity equations. However, since the $\nu_i^{predicted}$ were fit to experimental frequency shifts, $\nu_i^{observed}$, expressed in correct units, the omitted factor, M, in the predicted shifts forced the best fit "elastic constants" to differ from actual elastic constants by a factor M^{-2}. The

best fit parameters will henceforth be denoted by c^*_{mn}. The c^*_{mn} were significant in that they could be used to show interrelationships among the actual elastic constants, while possessing considerably less uncertainty in their values. The elastic constants were given in terms of the c^*_{mn} by:

$$c_{mn} = \frac{\lambda^2 \rho}{4n^2 \sin^2(\alpha/2)} \, c^*_{mn} \qquad 4\text{-}3$$

A Fortran computer program was used to perform an iterative procedure (see McLaren, 1973) which minimized χ^2 and yielded the c^*_{mn}. The K'th step in the iteration involved adding a quantity $\Delta c^{(K)}_{mn}$ to each of the parameters $c^{(K-1)}_{mn}$ estimated in the previous iteration step. The initial estimates, $c^{(0)}_{mn}$, could be specified more or less arbitrarily, but computer time was saved if they were chosen to lie near the anticipated values of the c^*_{mn}. The quantities $\Delta c^{(K)}_{mn}$ were calculated explicitly, using the $c^{(K-1)}_{mn}$ and an expression involving first and second partial derivatives of χ^2 with respect to the c_{mn}. The expression (see McLaren, 1973) was derived from a Taylor series expansion of the equations, $\frac{\partial(\chi^2)}{\partial c_{mn}} = 0$, which formed necessary conditions for a critical point of χ^2. After each iteration step, a new value for χ^2 was calculated and compared with the value obtained in the previous step. The iteration procedure was terminated when a step failed to yield a significant decrease in χ^2.

The design of the above mentioned Fortran program allowed only four parameters (c_{11}, c_{12}, c_{33} and c_{44}) to be varied independently when making the least squared fit. The fifth parameter, c_{13}, was specified as a linear function of the other parameters using a relationship (to be discussed in

detail in the following section) known to be valid for certain hexagonal crystals, in particular, for solid H_2 and β-N_2. The analysis of the Brillouin spectra of these two substances motivated the original construction of the program. The program required modification before it could be used to analyze the present data since evidence implying that the elastic constants of β-CO satisfied the relationship referred to above, could not be found in the literature. Hence, a trial numerical value of c_{13} was entered into the program, which then varied the other four parameters to yield a least squares fit. Subsequently, computer runs were made with different trial values of c_{13}. The final set of least squares parameters was taken from the run which yielded an overall minimum in χ^2. The values of the c^*_{mn} were thus determined to be:

$c^*_{11} = 2.473 \times 10^{19} \pm .2\%$ $\qquad$ $c^*_{12} = 1.490 \times 10^{19} \pm .5\%$

$c^*_{13} = 1.237 \times 10^{19} + .4\%$ $\qquad$ $c^*_{33} = 2.725 \times 10^{19} \pm .3\%$

$c^*_{44} = .461 \times 10^{19} \pm .8\%$

It should be noted that the above quantities are not elastic constants and are not expressed in any conventional units (dimensions are Hz^2). They are, however, related to the elastic constants of β-CO by the expression 4-3. The theoretical frequency shift curves specified by the above parameters, along with the experimental data points, are plotted in figure 8.

The errors indicated in the c^*_{mn} were calculated empirically, that is, they were determined entirely by the quality of the least squares fit. They reflect uncertainties in both the measured frequency shifts of the Brillouin components and in the orientation of the crystal. The errors were calculated by the Fortran program (for reasoning and formulas, see Landheer,

Figure 8 - Curves showing frequency shift, Ω, versus angle between wavevector and crystal c axis, γ, for the three components in the Brillouin spectrum of β - CO. Solid dots designate experimentally observed frequency shifts. Analogous curves for β - N_2 (inset; reproduced from paper by Kiefte and Clouter, 1976) are shown for purposes of comparison.

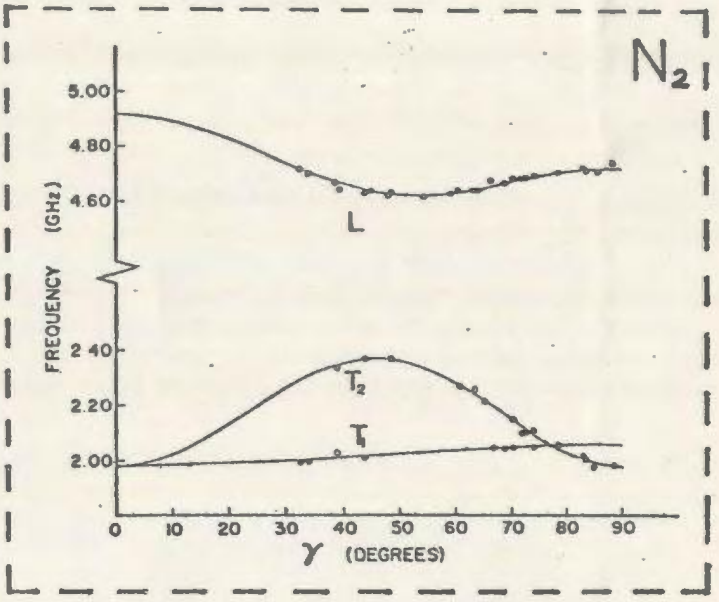
N2
5.00
4.80
4.60
2.40
2.20
2.00
FREQUENCY (GHz)
L
T2
T1
0 10 20 30 40 50 60 70 80 90
γ (DEGREES)

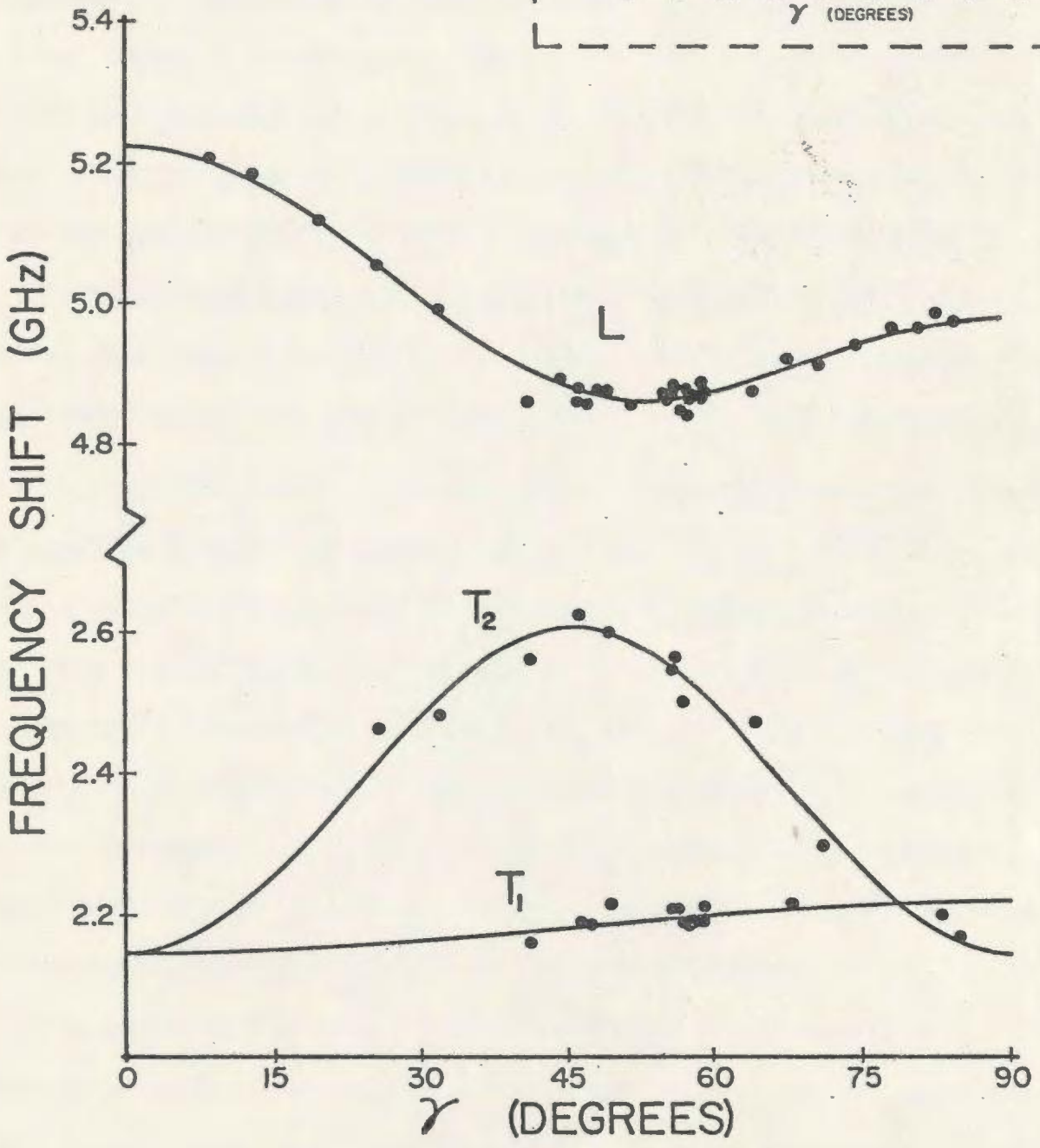
5.4
5.2
5.0
4.8
2.6
2.4
2.2
FREQUENCY SHIFT (GHz)
L
T2
T1
0 15 30 45 60 75 90
γ (DEGREES)

Figure 8

1974) with the uncertainty in a given parameter being defined as the square root of its empirical covariance. The uncertainties in the c^*_{mn} therefore corresponded to a single standard deviation. The validity of the error computations depended on having reasonable values for the standard deviations, σ_i (as in equation 4-1), of the experimental measurements. No attempt was made to determine the σ_i's in advance of the final analysis of the data. However, it was assumed that the σ_i's were all approximately equal (i.e. $\sigma_i \equiv \sigma$ for all i), since there did not appear to be any practical criterion for determining the relative accuracies of the various frequency shift measurements. The absolute error, rather that the percentage error, was assumed to be constant as there was no indication that the uncertainty in a frequency shift should be proportional to the magnitude of the shift. The value of σ was chosen to make $\chi^2_{minimum}$ (that is, the value of χ^2 obtained at the conclusion of the least squares fit) equal to 1 since the expectation value of $\chi^2_{minimum}$ is 1 when σ is 1 standard deviation (Landheer, 1974). The final analysis yielded σ = .017 GHz. This indicated that a frequency shift measured on the DAS multichannel analyzer had a standard deviation of .54 channels. The majority of this uncertainty was likely due to the inherent "roundoff" error caused by recording frequency shifts in terms of whole numbers of MCA channels. The largest deviation of any measured frequency shift from the appropriate predicted value was .043 GHz or 2.5 standard deviations.

To complete the analysis of the data and hence determine the elastic constants of β-CO, it was necessary to obtain values for the quantities λ, α, ρ and n appearing in equation 4-3. The laser wavelength, λ, was

Table 2

Physical Properties of β - CO (at triple point)

triple point temperature		68.15K	1
vapour pressure		115 mm	1
crystal structure		hcp ($P6_3/mmc$)	2
lattice parameters	a =	.414 nm	
	c =	.685 nm	3
	c/a =	1.65	
density		911 kg/m^3	4
refractive index (632.8 nm)		1.25	4
β - α transition temperature		61.55K	1

References:

1) Timmermans (1950)

2) Kohin (1960)

3) Barrett and Meyer (1965); Values for a and c given in this reference are from x-ray measurements made at 63K. The values were corrected to yield the appropriate triple point density assuming isotropic thermal expansion.

4) Section 2, Chapter 4, this thesis

5.1454×10^{-7} m, accurate to better than 1 part in 10^4. The uncertainty in the wavelength was small enough to allow λ to be treated as an exact parameter. The scattering angle, α, was set at 90^o using the procedure described in section 3, chapter 3. This procedure enabled α to be established (over the entire duration of the experiment) to within an uncertainty of about $.5^o$. The term $\sin^2(\alpha/2)$ appearing in equation 4-3 thus had a value of .5± .9%.

No directly measured value for the density, ρ, of β-CO at the triple point could be found in the literature. However, a paper by Fukushima, Gibson and Scott (1977) gave a value, 2.5 ± 8% cm^3/mole, for the molar volume decrease when carbon monoxide solidified at the triple point. In addition, a value for the density of liquid CO at the triple point could be calculated from a 16 parameter equation of state given in the National Bureau of Standards Technical Note No. 202 (Hust and Stewart, 1963). The equation, representing a least squares fit to a large variety of experimental thermodynamic data on liquid and gaseous CO, was specified to be accurate to within 1%. The calculated liquid density at 68.14 K, 115.1 mm Hg was 842.9 ± 1% kg/m^3. A measured value for the density (847.1 kg/m^3 at 68.12 K, 115.1 mm Hg) was also available (Timmermans, 1950) but this was not used here as it did not include a stated uncertainty. Combining the molar volume decrease with the calculated liquid density yielded the value, ρ = 911 ± 1.3% kg/m^3 for the density of solid CO at the triple point.

A search of the literature did not reveal any values whatsoever for the refractive index, n, of either liquid or solid CO. An experiment* was

* The experiment was performed by Mr. Robert Gagnon, undergraduate student at the Memorial University of Newfoundland, as part of his honours thesis work.

thus undertaken to determine the index of refraction of the liquid, with the assumption that a value for the solid could then be obtained with the aid of the Lorentz-Lorenz relation. The experiment involved condensing a sample of carbon monoxide in a liquid nitrogen cooled precision rectangular quartz cell. This was housed in a vacuum insulated cryostat which allowed the cell to be rotated about a vertical axis and permitted optical access to the cell by way of two glass windows. The refractive index was measured by an interference technique in which a beam from a helium-neon laser was split into two closely spaced parallel beams, one of these passing through the cell and the other just missing it. The beams were reflected by a mirror and sent back through the cryostat a second time before being recombined by the same beam splitter that originally separated them. The cell was rotated by an electrically driven mechanism synchronized with a chart recorder. The rotation changed the optical path through the rectangular cell and thereby caused the intensity of the recombined laser beam to vary according to whether constructive or destructive interference occurred. Variations in the intensity were photoelectrically monitored and traced by the chart recorder. Since the angles of rotation corresponding to observed intensity maxima were dependent on the index of refraction of the cell contents, the index could be fit to the experimental data with the aid of a least squares routine. The required routine was programmed on an SR-52 calculator. The value for n obtained in the experiment was 1.22, this then being the refractive index for 632.8 nm light in liquid CO at 77.4 K (the normal boiling point temperature of N_2).

The error in n could only be estimated roughly, as the experiment on

carbon monoxide was performed just once. However, in the initial testing of the apparatus, experiments were run on other materials (namely methanol and liquid oxygen) with known refractive indices and the results were found to be accurate to within at least 1.5%. This value was thus taken to be the uncertainty in the measurement on carbon monoxide. Since the wavelength used in measuring the refractive index differed from the wavelength used in the Brillouin scattering experiment, an additional uncertainty in n had to be included to allow for the effects of dispersion. Measurements of the refractive indices of the liquids O_2, N_2 and H_2 (Johns and Wilhelm, 1937) at three wavelengths show maximum variations of less than .5% over the relevant wavelength range. An error of .5% was thus added to the 1.5% error mentioned above to yield an uncertainty of 1.6% in the value of n. No additional uncertainty was included to allow for possible effects of birefringence in crystalline CO as, by analogy with nitrogen (Kiefte and Clouter, 1976), birefringence was assumed to be negligible.

The refractive index of β-CO at the triple point was calculated from the value of 77.4 K using the Lorentz-Lorenz relation (Jackson, 1975):

$$\frac{n^2-1}{n^2+2} = \frac{\rho}{\rho'} \frac{n'^2-1}{n'^2+2} \qquad 4\text{-}4$$

In equation 4-4, ρ' and ρ denote the densities of CO at 77.4 K and β-CO at the triple point respectively. The quantity, n', is the refractive index at 77.4 K and n is the index for the solid at the triple point. A value for ρ' at 77.4 K, 760 mm Hg was calculated using the carbon monoxide

equation of state (Hust and Stewart, 1973) referred to previously. The value was found to be $\rho' = 807 \pm 1\%$ Kg/m^3. Calculating n from equation 4-4 using the above determined magnitudes and uncertainties for the various parameters, yielded $n = 1.25 \pm 1.8\%$.

With the values for λ, α, ρ and n specified above, it is possible to calculate the multiplicative parameter linking the previously determined c^*_{mn} to the elastic constants of β-CO. In S.I. units, this parameter is found to be:

$$\frac{\lambda^2 \rho}{4n^2 \sin^2(\alpha/2)} = 7.72 \times 10^{-11} \pm 3.9\%$$

Hence:

$$c_{mn} = (7.72 \times 10^{-11} \pm 3.9\%)\ c^*_{mn} \text{ newtons/m}^2$$

The stated error includes the above determined uncertainties in the scattering angle, density and refractive index. By far the major contribution to the error comes from the refractive index (3.6% uncertainty in n^2) and it is hoped that a more accurate measurement of this parameter will be obtained shortly.

The elastic constants of β-CO at 67.6 K (.5 K below the triple point) are determined to be:

$$\left.\begin{aligned} c_{11} &= 1.909 \pm .2\% \\ c_{12} &= 1.151 \pm .5\% \\ c_{13} &= .955 \pm .4\% \\ c_{33} &= 2.104 \pm .3\% \\ c_{44} &= .356 \pm .8\% \end{aligned}\right\} \times 10^9 \pm 3.9\%\ \text{N/m}^2$$

(uncertainty in temperature = .2 K)

The above values are adiabatic elastic constants, that is, they are appropriate for deformations occuring at constant entropy. Isothermal (constant temperature) elastic constants are related to the above values by an expression (Nye, 1957) involving the heat capacity and thermal expansion tensor for β-CO. Throughout the following section (i.e. section 4, chapter 4) all values quoted for elastic constants and for quantities derived from elastic constants will be the adiabatic values.

4.3 Discussion

The elastic constants determined in this investigation can be related to a variety of physical properties of the β-carbon monoxide crystal. These properties, along with the values of the elastic constants themselves form a basis for comparing and contrasting β-CO with other materials. By far the most interesting comparison would appear to be with β-N_2, which was found to have elastic properties very similar to those of β-CO. However, a comparison of β-CO with hcp hydrogen is also useful due to the similarities in the molecules and in the crystal structures of the two materials. For purposes of contrast, brief mention will be made of the elastic properties of ice and beryllium. Both of these substances form hexagonal crystals (beryllium is hcp, ice is not hcp) but needless to say their molecular interactions and consequently their elastic properties, are fundamentally different from those of β-CO. A list of the elastic constants of the five substances mentioned above appears in table 3.

One of the simplest physical properties derivable from the elastic

Table 3

Elastic constants of five hexagonal crystals

Material	c/a	c_{11}	c_{12}	c_{13}	c_{33}	c_{44}	Bulk Modulus	ref
		(in units of 10^9 newtons/m^2)						
β - CO (67.6K)	1.65	1.909	1.151	.955	2.104	.356	1.338	1
β - N_2 (63K)	1.63	1.825	1.131	.980	1.976	.320	1.312	2
H_2 (13.2K)	1.63	.334	.130	.056	.408	.140	.173	3
Ice (257K)	—	13.20	6.69	5.84	14.42	2.89	8.617	4
Be	1.58	308	-58	87	357	110	120	5

References:

1) present work

2) Kiefte and Clouter (1976)

3) Thomas et al. (1977)

4) Hobbs (1974)

5) AIP Handbook (1972)

constants is the volume compressibility, C. This is defined as the fractional decrease in volume of a crystal under hydrostatic pressure. That is,

$$C = -\frac{1}{V}\frac{\partial V}{\partial P} \qquad 4\text{-}5$$

where the volume of the crystal is V and the stress tensor designating hydrostatic pressure is given by:

$$\sigma_{ij} = -P\,\delta_{ij} \qquad 4\text{-}6$$

C can be expressed in terms of the elastic constants by using Hooke's law to determine the strain tensor induced by hydrostatic pressure, and then calculating the volume decrease implied by the strain. For hexagonal crystals, C is found to be (using formulas given in Nye, 1957):

$$C = \frac{c_{11} + c_{12} - 4\,c_{13} + 2\,c_{33}}{(c_{11} + c_{12})\,c_{33} - 2\,c_{13}^2} \qquad 4\text{-}7$$

The reciprocal of C is known as the bulk modulus, B, and is a direct measure of the resistance to compression of a crystal lattice. The bulk moduli of β-CO, β-N_2, H_2, ice and Be are given in table 3 . The values of the bulk moduli show a variation over three orders of magnitude between H_2 and Be, with β-CO lying near the low end of the range. Low bulk moduli are characteristic of van der Waals lattices (that is, lattices composed of molecules interacting primarily by van der Waals forces) of which CO, N_2 and H_2 are examples. Other van der Waals lattices, notably O_2 (Kiefte and Clouter, 1975), and the rare gas solids, Ar, Ne, Kr and Xe (Stoicheff,

1977) all have bulk moduli of roughly the same order of magnitude as β-CO. The bulk modulus of Be is typical of that of many metals.

Another readily computed elastic property of crystals is the linear compressibility, β. This quantity is defined to be the fractional decrease in the length of a line in a crystal when the crystal is subjected to hydrostatic pressure. That is,

$$\beta = -\frac{1}{\ell}\frac{\partial \ell}{\partial P} \qquad 4\text{-}8$$

where ℓ is the length of a line fixed in a crystal and P is the hydrostatic pressure. In general, β depends on the direction of the line, ℓ, relative to the crystal geometry. For hexagonal crystals, a method analogous to that used in calculating the volume compressibility yields (by way of formulas given in Nye, 1957),

$$\beta = \beta_1 + \beta_2 \cos^2\gamma \qquad 4\text{-}9$$

where

$$\beta_1 = \frac{c_{33} - c_{13}}{(c_{11} + c_{12})\, c_{33} - 2\, c_{13}^2}$$

$$\beta_2 = \frac{c_{11} + c_{12} - c_{13} - c_{33}}{(c_{11} + c_{12})\, c_{33} - 2\, c_{13}^2}$$

γ = angle between ℓ and hexagonal axis

For β-carbon monoxide the coefficients β_1 and β_2 in equation 4-9 are found

to be, $\beta_1 = 2.49 \pm .1 \times 10^{-10}$ m^2/N and $\beta_2 = 0.00 \pm .02 \times 10^{-10}$ m^2/N.* This yields the result that, to within the experimental uncertainty, the linear compressibility of β-CO is isotropic. Thus, a lump of β-CO would, when exposed to hydrostatic pressure, change in volume but not in shape. In this respect, β-CO resembles a cubic crystal where symmetry considerations necessitate isotropy in the linear compressibility. An equivalent way of stating the above experimental result is to say that the ratio, c/a, of the β-CO crystal lattice parameters, is found to be independent of pressure. The simple argument showing the equivalence of the two statements runs as follows:

$$\frac{\partial}{\partial P}\left(\frac{c}{a}\right) = -\frac{c}{a}\left(-\frac{\partial c}{c\partial P} + \frac{\partial a}{a\partial P}\right)$$

$$= -\frac{c}{a}\left(\beta(\gamma = 0^o) - \beta(\gamma = 90^o)\right)$$

$$= -\frac{c}{a}\beta_2$$

Thus, for $\beta_2 = 0$, $\frac{c}{a}$ is independent of pressure. The result is not surprising for the case of hexagonal close packed crystals (like β-CO) since it is a consequence of assuming that the spheres forming the close packed arrangement remain spherical under pressure. Invariance of the c/a ratio was a prior assumption used in analyzing Brillouin data to obtain the elastic constants of β-N_2 (Kiefte and Clouter, 1976) and H_2 (Landheer, 1974). Experimental evidence (actual measurements of the axis ratio at different pressures) substantiating the assumption was available for both those materials, thus,

*The elastic constants were treated as independent random variables for purposes of estimating the error in the various derived quantities.

justifying analysis of the data subject to the restriction:

$$c_{11} + c_{12} - c_{13} - c_{33} = 0 \qquad 4\text{-}10$$

This restriction was the one, mentioned in the previous section, which allowed the computer program to be written so as to fit only four, rather than five, independent parameters to the experimental data. Equation 4-10, although verified here in the final results, could not be used as a prior assumption since no investigation of the axis ratio dependence on pressure, has been reported for β-carbon monoxide. Calculations using the elastic constants of ice and beryllium show that the linear compressibility is within 5% of being isotropic in ice but is highly anisotropic in Be. In fact, the linear compressibility of Be in the $\gamma = 90^{o}$ direction is about 3.5 times that in the $\gamma = 0^{o}$ direction. These results point out that isotropic linear compressibility in a hexagonal crystal is not necessarily related to the crystal having a close packed structure. The observed isotropy in the linear compressibility of β-CO, β-N_2 and H_2 is an important similarity in the properties of crystals of these substances.

Further similarity in the elastic properties of β-CO, β-N_2 and H_2 arises from considering Young's modulus, E, for the three materials. Young's modulus is defined as the ratio of longitudinal stress to longitudinal strain and, physically, it reflects the tension required to induce a given proportional change in length of a rod cut from a single crystal. Like the linear compressibility, Young's modulus, in general depends on direction (i.e. the direction of the axis of the rod relative to the crystal

geometry). It can be calculated in a manner analogous to the procedure used in calculating the volume compressibility and for hexagonal crystals, is found to be (using formulas given in Nye, 1957),

$$E^{-1} = R \sin^4\gamma + S \cos^4\gamma + T \sin^2\gamma \cos^2\gamma \qquad 4\text{-}11$$

where

$$R = \frac{c_{11}\, c_{33} - c_{13}^2}{(c_{11}^2 - c_{12}^2)\, c_{33} - 2\,(c_{11} - c_{12})\, c_{13}^2}$$

$$S = \frac{c_{11} + c_{12}}{(c_{11} + c_{12})\, c_{33} - 2\, c_{13}^2}$$

$$T = \frac{(c_{11} + c_{12})\, c_{33} - 2\,(c_{13} + c_{44})\, c_{13}}{(c_{11} + c_{12})\, c_{33}\, c_{44} - 2\, c_{13}^2\, c_{44}}$$

For β- carbon monoxide, Young's modulus is determined by:

$$R = .8876 \qquad S = .6632 \qquad T = 2.395$$

E has a maximum value of 1.508×10^9 N/m^2 at $\gamma = 0^o$ and a minimum value of $.999 \times 10^9$ N/m^2 at $\gamma = 52.7^o$. Not surprisingly, the curve generated by plotting E vs. γ has an overall shape similar to that of the frequency shift vs. γ curve for the longitudinal Brillouin component (see figure 8). However, the anisotropy apparent in Young's modulus (maximum E is 50% greater than minimum E) is substantially greater than the anisotropy in the velocity of propagation of longitudinal elastic waves. In fact, Young's modulus is

one of the most highly anisotropic elastic properties of the β-carbon monoxide crystal.

Young's modulus for β-N_2 is very similar to that for β-CO. The parameters determining the dependence of E on γ for β-N_2 are:

$$R(N_2) = .9725 \qquad S(N_2) = .7540 \qquad T(N_2) = 2.625$$

The primary difference in the E vs. γ curves for β-CO and β-N_2 is simply a multiplicative constant. That is, $E(N_2) \simeq .91\ E\ (CO)$, this relation holding to within 3.4% over the full range of γ and to within .4% for $\gamma > 45^o$. The minimum value of E for β-N_2 is $.908 \times 10^9$ N/m^2, occurring at $\gamma = 52.1^o$. The E vs. γ curve for H_2 is also quite similar to the curve for β-CO but the H_2 values are lower by a factor of about .26. The direction of minimum E in H_2 is $\gamma = 55.4^o$. Ice yields much higher values of Young's modulus than does β-CO and has a considerably smaller range of percentage variation in E. However the shape of the E vs. γ curve for ice is roughly similar to the CO, N_2 and H_2 curves. Beryllium on the other hand shows a totally different dependence of E on γ with E being much more nearly isotropic and having a minimum at $\gamma = 90^o$. As well, Young's modulus in beryllium is about 200 times greater than that in β-carbon monoxide.

As is apparent from inspecting the curves shown in figure 8, the dependence of elastic wave propagation velocities (or, equivalently, Brillouin frequency shifts) on γ is very similar for the crystals, β-CO and β-N_2, but the velocities average about 4% lower in β-N_2. In both β-CO and β-N_2, the velocity of the T1 component increases monotonically with

γ. The reverse situation occurs in solid H_2, where the T1 velocity decreases monotonically as γ increases. An absolute minimum in the longitudinal wave velocity occurs at $\gamma = 53.3^o$ in β-CO, compared with $\gamma = 52.8^o$ in β-N_2 and $\gamma = 55.2^o$ in solid H_2. CO, N_2 and H_2 crystals all show absolute maxima in their T2 wave velocities in the neighbourhood of $\gamma = 45^o$. The precise locations of the maxima are at $\gamma = 45.9^o$ for β-CO, $\gamma = 45.8^o$ for β-N_2 and $\gamma = 47.5^o$ for H_2. There are directions in both β-CO and β-N_2 along which the two transverse components have equal propagation velocities. These directions correspond to the crossing over of the T1 and T2 curves which is apparent in figure 8. The crossover occurs at $\gamma = 79.1^o$ in β-CO and at $\gamma = 77.1^o$ in β-N_2. No crossover occurs in H_2 where the propagation velocity of the T1 component is lower than that of the T2 component for the full range of γ. The fact that the two transverse components have equal velocities when $\gamma = 0^o$ in both β-CO and in β-N_2, is reflected in of the form of the equations 1-39 and is a result which holds for all hexagonal crystals. Similarily, in all hexagonal crystals, the velocity of the T2 component in the $\gamma = 0^o$ direction equals the T2 velocity in the $\gamma = 90^o$ direction.

The conditions required for complete elastic isotropy in a hexagonal crystal are:

$$\begin{aligned} c_{11} &= c_{33} \\ c_{12} &= c_{13} \\ 2c_{44} &= c_{11} - c_{12} \end{aligned} \qquad 4\text{-}12$$

These relations are readily derived using the criterion that the γ dependence

be eliminated from the velocity equations, 1-39. Needless to say, the equations 4-12 do not hold for β-CO. The discrepancies are of the order of 10% to 20%.

The above discussion has dealt with most of the intuitively significant and easily derived elastic properties of β-CO at the triple point. The similarity of the various properties with those of β-N_2 is quite remarkable. Some properties, notably the bulk modulus, the linear compressibility and the magnitudes of some of the individual elastic constants, agree to within the experimental uncertainty. On the other hand, Young's modulus in β-N_2 is lower than that in β-CO by a fraction which lies outside the experimental error. As well, β-CO and β-N_2 show significant differences in some dimensionless quantities derived from ratios of expressions involving elastic constants. These ratios, for example, Young's modulus ÷ bulk modulus or, velocity of T2 wave ÷ velocity of L wave, have relatively small uncertainties and hence provide sensitive tests for similarities in elastic properties. The small but nevertheless distinct dissimilarities in the elastic behaviour of β-CO and β-N_2 should provide important clues as to the differences in the molecular interactions in these two substances. At the same time, the overall similarity in properties facilitates the drawing of detailed and useful analogies between the two materials. In this light, it is hoped that an investigation of the elastic aspects of the β-α phase transition in solid CO will, as a bonus, provide substantial insight into the analogous transition in N_2. The present work forms the preliminary step in the above mentioned investigation, the major portion of which will be commenced shortly.

APPENDIX 1

TABLE OF 4δ (δ ≡ INTERPLANAR ANGLE) VERSUS PAIRS OF FORMS, $\{h_1k_1l_1\}$ - $\{h_2k_2l_2\}$, FOR HCP CRYSTALS.

Forms considered in the table are: {001}, {100}, {101}, {110}, {201}, {301}, {120}, {102}, {103}, {130}, {111}, {112}, {121}

4δ	Forms	4δ	Forms
1		41	
2		42	
3		43	
4		44	{110}-{120}
5		45	{120}-{121}, {102}-{103}
6		46	
7		47	
8		48	{111}-{121}
9		49	
10		50	{130}-{121}
11		51	
12		52	{101}-{201}
13		53	
14		54	
15		55	
16		56	{100}-{130}
17		57	
18		58	{111}-{112}
19	{201}-{301}	59	{100}-{201}
20		60	
21	{120}-{130}	61	
22		62	
23		63	{110}-{121}
24		64	{110}-{130}
25		65	
26		66	
27		67	
28		68	{110}-{111}, {130}-{301}
29		69	
30		70	
31		71	
32		72	{101}-{301}
33		73	
34		74	
35		75	{101}-{102}, {121}-{301}
36		76	{100}-{120}, {121}-{201}
37		77	
38		78	
39		79	
40	{100}-{301}	80	{120}-{121}, {301}-{301}

4δ	Forms
81	{130}-{201}
82	
83	
84	
85	{121}-{121}
86	{120}-{301}
87	{120}-{120}
88	{100}-{121}
89	
90	{121}-{112}
91	{121}-{121}
92	
93	{130}-{111}
94	
95	
96	{120}-{201}
97	
98	{120}-{121}, {101}-{121}
99	
100	{201}-{301}
101	
102	
103	
104	
105	{101}-{112}
106	
107	
108	{120}-{130}
109	
110	{102}-{112}
111	{130}-{130}
112	{100}-{101}
113	
114	{121}-{301}
115	
116	{130}-{121}, {111}-{201}
117	
118	
119	{101}-{111}, {201}-{201}
120	{100}-{110}, {101}-{103}, {111}-{301}
121	{111}-{121}
122	
123	{103}-{103}
124	{130}-{101}
125	{121}-{121}
126	{110}-{301}, {110}-{112}
127	{201}-{102}
128	{201}-{112}
129	{130}-{130}, {001}-{103}, {121}-{201}
130	
131	

4δ	Forms
132	{120}-{130}
133	{110}-{201}, {120}-{112}, {112}-{103}
134	{120}-{101}
135	
136	{100}-{111}, {111}-{111}
137	
138	
139	{130}-{121}
140	{130}-{112}, {301}-{112}
141	
142	
143	
144	
145	
146	
147	{301}-{102}
148	{102}-{103}
149	
150	{121}-{121}
151	
152	{101}-{301}
153	{120}-{120}
154	
155	{111}-{102}, {121}-{102}
156	
157	
158	{120}-{121}
159	
160	{110}-{101}, {121}-{201}, {102}-{102}
161	{111}-{301}, {121}-{301}
162	
163	
164	{100}-{120}
165	
166	
167	{101}-{121}
168	{120}-{301}
169	{100}-{121}
170	{100}-{112}
171	{101}-{201}
172	{120}-{201}, {201}-{103}
173	{001}-{102}
174	{101}-{121}, {111}-{201}
175	
176	{110}-{130}, {121}-{112}
177	{121}-{121}
178	
179	
180	
181	
182	
183	

4δ	Forms
184	{100}-{130}, {121}-{301}
185	
186	{130}-{111}, {111}-{103}
187	{100}-{102}
188	{130}-{301}
189	
190	
191	{111}-{121}, {301}-{103}
192	{120}-{101}, {130}-{201}
193	{130}-{102}, {121}-{201}
194	{111}-{112}
195	{121}-{103}
196	{110}-{120}
197	{121}-{102}
198	{120}-{102}, {121}-{112}
199	
200	{110}-{121}, {101}-{102}
201	
202	{301}-{112}, {112}-{112}
203	{101}-{103}
204	
205	{120}-{111}
206	
207	
208	{130}-{112}
209	{130}-{101}
210	{101}-{101}
211	
212	
213	
214	{110}-{102}, {101}-{111}
215	
216	
217	
218	{201}-{112}
219	{120}-{130}
220	{103}-{103}
221	
222	{130}-{121}
223	{101}-{121}
224	{120}-{112}, {101}-{101}, {111}-{112}, {121}-{103}
225	{111}-{121}
226	
227	{101}-{201}, {301}-{102}
228	{111}-{111}
229	
230	
231	{100}-{103}, {201}-{201}
232	
233	
234	{001}-{112}

4δ	Forms
235	{120}-{102}, {121}-{121}, {201}-{301}, {201}-{102}
236	{130}-{103}, {101}-{301}, {301}-{301}
237	
238	
239	{120}-{103}
240	{100}-{100}, {110}-{110}, {120}-{120}, {130}-{130}
241	
242	{100}-{301}, {121}-{102}
243	{120}-{121}
244	{100}-{201}
245	
246	{110}-{111}, {130}-{102}, {201}-{102}
247	{201}-{103}
248	{001}-{101}
249	{301}-{102}
250	{110}-{103}
251	
252	{301}-{301}, {112}-{112}
253	
254	{121}-{112}
255	{100}-{101}, {121}-{121}, {112}-{103}
256	
257	{102}-{103}, {103}-{103}
258	{201}-{301}
259	{110}-{112}
260	
261	{120}-{130}
262	
263	{130}-{121}, {301}-{103}
264	{101}-{112}
265	{120}-{103}, {201}-{201}
266	
267	
268	
269	
270	
271	{301}-{103}, {102}-{112}
272	{121}-{112}
273	{130}-{103}, {111}-{111}
274	{121}-{102}
275	{111}-{121}
276	
277	{101}-{301}, {111}-{102}
278	
279	
280	{100}-{102}
281	
282	
283	
284	{110}-{120}, {121}-{103}
285	{110}-{121}
286	

4δ	Forms
287	{120}-{111}
288	
289	{101}-{201}
290	
291	{201}-{103}
292	{001}-{111}, {102}-{102}
293	
294	
295	{120}-{112}
296	{100}-{130}
297	{130}-{301}, {121}-{102}
298	{100}-{103}, {130}-{201}, {101}-{102}
299	{121}-{103}
300	
301	{001}-{201}, {101}-{121}, {111}-{112}
302	{111}-{121}, {102}-{103}
303	{130}-{101}, {101}-{112}, {111}-{103}
304	{110}-{130}
305	
306	
307	{130}-{111}, {121}-{201}, {121}-{103}
308	
309	
310	{121}-{301}
311	{111}-{102}, {301}-{102}
312	
313	{130}-{112}
314	
315	{001}-{121}
316	{100}-{120}, {130}-{102}, {111}-{103}
317	{100}-{121}, {120}-{301}
318	{120}-{201}
319	{121}-{121}
320	{001}-{301}
321	{101}-{101}, {121}-{112}
322	{120}-{101}
323	{101}-{103}
324	
325	
326	{130}-{103}, {121}-{301}
327	{120}-{120}, {201}-{102}
328	{120}-{121}, {101}-{111}
329	{201}-{112}
330	{120}-{102}, {121}-{201}
331	{102}-{112}
332	
333	
334	{301}-{103}
335	
336	
337	{120}-{103}, {121}-{121}
338	

4δ	Forms
339	{301}-{112}, {112}-{112}
340	
341	
342	
343	{101}-{103}, {111}-{201}
344	{101}-{121}, {121}-{103}
345	
346	
347	{102}-{102}
348	{120}-{130}, {130}-{121}, {111}-{301}
349	{112}-{103}
350	
351	{130}-{130}, {101}-{102}, {201}-{103}
352	
353	
354	
355	
356	{121}-{102}
357	
358	
359	
360	{100}-{110}, {100}-{001}, {100}-{111}, {100}-{112}, {110}-{001}, {110}-{101}, {110}-{201}, {110}-{301}, {110}-{102}, {110}-{103}, {120}-{001}, {130}-{001}

References

American Institute of Physics Handbook, Third Edition (1972).

Azaroff, L.V., Elements of X-ray Crystallography (McGraw-Hill, New York, 1968).

Barrett, C. S. and L. Meyer, J. Chem. Phys., 43, 3502 (1965).

Benedek, G. B. and K. Fritsch, Phys. Rev., 149, 647 (1966).

Born, M. and K. Huang, Dynamical Theory of Crystal Lattices (Clarendon Press, Oxford, 1954).

Born, M. and E. Wolf, Principles of Optics (Pergamon Press, New York, 1964).

Burleigh Instruments Inc., "Technical Memorandum for Fabry-Perot Interferometry", No. FP 140475 (1976).

Cullity, B. D., Elements of X-ray Diffraction (Addison-Wesley, Reading, Ma., 1956).

Fukushima, E., A. A. V. Gibson and T.A. Scott, J. Low Temp. Phys., 28, 157 (1977).

Gewurtz, S. and B. P. Stoicheff, Phys. Rev. B, 10, 3487 (1974).

Goldman, V. V. and M. L. Klein, J. Chem. Phys., 64, 5121 (1976).

Goldstein, H., Classical Mechanics (Addison-Wesley, Cambridge, 1950).

Gornall, W. S. and B. P. Stoicheff, Phys. Rev. B, 4, 4518 (1971).

Hobbs, P. V., Ice Physics (Clarendon Press, Oxford, 1974).

Hust, J. G. and R. B. Stewart, Technical Note 202 (U.S. National Bureau of Standards, Washington, D.C., 1963).

Jackson, J. D., Classical Electrodynamics (John Wiley and Sons, Inc., New York, 1975, 2nd. Edition).

Jenkins, F. A. and H. E. White, Fundamentals of Optics (McGraw-Hill, New York, 1957).

Johns, H. E. and J. O. Wilhelm, Can. J. Res., 15, 101 (1937).

Kiefte, H. and M. J. Clouter, J. Chem. Phys., 63, 3863 (1975).

Kiefte, H. and M. J. Clouter, J. Chem. Phys., 64, 1816 (1976).

Kittel, C., Introduction to Solid State Physics (John Wiley and Sons, Inc., New York, 1976, 5th. Edition).

Klein, M. L. and J. A. Venables, Rare Gas Solids, Vol. II, (Academic Press, New York, 1977).

Kohin, B. C., J. Chem. Phys., 33, 882 (1960).

Landau, L. D. and E. M. Lifshitz, Theory of Elasticity (Addison-Wesley, Reading, Ma., 1959).

Landheer, D., Ph.D. Thesis, University of Toronto, 1974 (Unpublished).

Landheer, D., H. E. Jackson, R. A. McLaren and B. P. Stoicheff, Phys. Rev. B, 13, 888 (1976).

McLaren, R. A., Ph.D. Thesis, University of Toronto, 1973 (Unpublished).

McLaren, R. A., H. Kiefte, D. Landheer and B. P. Stoicheff, Phys. Rev. B, 11, 1705 (1975).

Musgrave, M. J. P., Crystal Acoustics, (Holden-Day, San Francisco, 1970).

Nye, J. F., Physical Properties of Crystals (Clarendon, Oxford, 1957).

Sandercock, J. R., in: Proceedings of the Second International Conference on Light Scattering in Solids, edited by M. Balkanski (Flammarion Sciences, Paris, 1971).

Scott, T. A., Physics Reports (Section C of Physics Letters), 27, 89 (1976).

Stoicheff, B. P., in: Rare Gas Solids, Vol. II, edited by M. L. Klein and J. A. Venables (Academic Press, New York, 1977).

Thomas, P. J., S. C. Rand, D. Landheer and B. P. Stoicheff, Presentation No. ThE12, Optical Society of America Annual Meeting (1977).

Timmermans, J., Physico-Chemical Constants of Pure Organic Compounds (Elsevier, New York, 1950).